Chapter 2
Molecules in Strong Laser Fields

The purpose of this chapter is to provide the background and context for interpreting the experiments presented in this thesis. In particular, they aim at understanding the internal dynamics of CO_2 induced by a strong laser field. For a scientist (and especially for a Ph.D. student), this is a rather worrying prospect. Due to the complexity of molecular systems there are usually several mechanisms contributing to one particular outcome. This complicates the interpretation of the experimental results. Often, quantitative numerical simulations can help resolve this issue. However the strong laser field distorts the molecular system significantly and only adds to its complexity. This renders quantitative calculations a challenging problem, usually requiring a (second?) Ph.D. in computational physics. This thesis attempts to escape from this dilemma by measuring the molecular dynamics as a function of many different laser parameters. In this way, the dominating mechanism may be identified, enabling a qualitative understanding of the results. This chapter is thus focussed on introducing the studied strong field processes (ionisation, double ionisation and dissociation) and their dependence on the laser parameters (intensity, wavelength, polarisation and ellipticity). Emphasis is placed on available experimental results where possible.

2.1 Atoms in Strong Laser Fields

As molecules are composed of atoms, it is helpful to start with their response to a strong electric field. When near-infrared radiation is used as in the experiments discussed in this thesis, the corresponding *strong field regime* is roughly characterised by the onset of *ionisation*—the removal of an electron from the atom. In the following sections, the possible ionisation pathways are discussed in more detail, before looking at the interaction of the freed electron with the remaining laser field.

M. Oppermann, *Resolving Strong Field Dynamics in Cation States of CO_2 via Optimised Molecular Alignment*, Springer Theses, DOI: 10.1007/978-3-319-05338-7_2,

2.1.1 The Strong Field Regime

The ionisation potential I_p of an atom is defined as the energy required to lift its most loosely bound electron into the continuum (a bound-continuum transition). When irradiated by light of sufficiently high frequency ω, this is possible via a single-photon transition [1]. Yet, ionisation is also possible in lower frequency fields. Here, ionisation takes place via the absorption of n photons of energy $\hbar\omega$, such that $(n-1)\hbar\omega < I_p < n\hbar\omega$. This was first observed in 1965 by Voronov and Delone, involving a seven-photon transition in Xenon [2]. The corresponding multiphoton ionisation (MPI) rate can be obtained by treating the field as a small perturbation with respect to the Coulomb potential of the atom [3]. The associated theoretical framework is called lowest order perturbation theory (LOPT) and results in an intensity scaling that takes the form of a power law:

$$\Gamma_n^{(MPI)} = \sigma_n I^n \tag{2.1}$$

where σ_n is the n-photon absorption cross-section and I the light intensity. However, with increasing intensity, higher order terms become significant requiring an extension of LOPT. In 1979 Agostini et al. then observed MPI transitions with additional excess or *above threshold* photons [4]. This is illustrated in part (a) of Fig. 2.1. These continuum-continuum transitions increase the freed electron's kinetic energy. The MPI rate of an $(n+s)$-photon transition thus scales in intensity to the power of (n + s). This has been verified in an intensity range up to $10^{12}\,\mathrm{W\,cm^{-2}}$ [5]. However, the observation of high order above threshold ionisation usually requires intensities on the order of $10^{13}\,\mathrm{W\,cm^{-2}}$, due to the fast decrease of the absorption cross-section with the photon number. Here, the oscillatory laser field becomes strong enough to couple to the atomic states [6]. This effect is called the AC-Stark shift and becomes stronger with increasing intensity and the more loosely the electron is bound in the atom. One may estimate an upper limit of the associated energy level shift by treating the most weakly bound electron as freely oscillating in the laser field. This approximation is appropriate for atomic Rydberg states, for example. It thus approximately acquires the cycle averaged quiver energy of a free electron in an AC-field, called the ponderomotive potential U_p. Given a laser field of the form $E_L(t) = E_L \sin(\omega_L t)$, the electron's acceleration then is $a(t) = \dot{v}(t) = \frac{e}{m_e} E_L(t)$, such that [3]:

$$U_p[eV] = \left\langle \frac{1}{2} m_e v(t)^2 \right\rangle = \frac{(eE_L)^2}{4 m_e \omega_L^2} \approx 9.33 \times 10^{-14} I[\mathrm{W\,cm^{-2}}] \lambda^2[\mu\mathrm{m}] \tag{2.2}$$

where m_e is the electron's mass and λ the laser wavelength. The effective ionisation potential is thus increased by this energy (see part (a) of Fig. 2.1), leading to a reduction of the ejected electron's kinetic energy by the same amount:

$$E_{kin} \approx (n+s)\hbar\omega - (I_p + U_p) \tag{2.3}$$

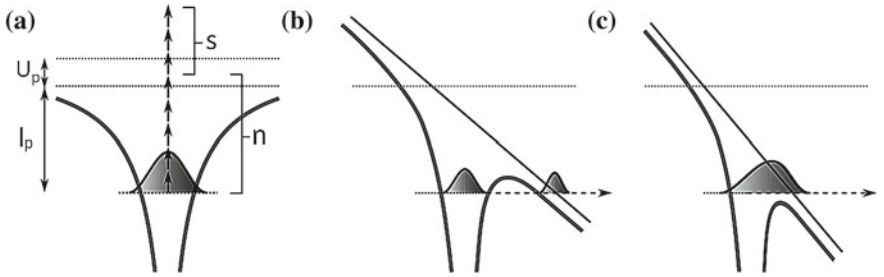

Fig. 2.1 Ionisation scenarios in the strong field regime: multiphoton ionisation (**a**), tunneling ionisation (**b**) and over-the-barrier ionisation (**c**)

where s is the number of excess photons. Once the ponderomotive energy becomes larger than the photon energy, entire peaks in the low kinetic energy region of the above-threshold ionisation (ATI) spectra are suppressed [7]. For this, the laser field cannot be treated as a perturbation anymore and LOPT treatment together with the multiphoton picture begins to fail. Approaching laser intensities on the order of $10^{14}\,\mathrm{W\,cm^{-2}}$ this also becomes apparent through another feature in atomic ATI. Here, Paulus et al. were the first to observe a plateau in the ATI spectra, associated with an almost constant ionisation probability over an extended range of high order ATI transitions [8, 9]. As LOPT leads to a strong exponential decrease of the ionisation cross-section with the ATI order, perturbation theory fails and a non-perturbative treatment is required. This was first realised by Keldysh in 1965 via a semiclassical model that treats the laser field classically [10]. Due to its non-perturbative interaction with the atom's Coulomb potential a barrier of finite width is formed. This allows the build-up of a tunneling current, resulting in field ionisation. This mechanism is thus called *tunneling ionisation* (TI) and is illustrated in part (b) of Fig.2.1. MPI and TI represent the limiting cases of ionisation in a strong laser field, however there is no sharp transition between them at a particular intensity.

Keldysh developed an adiabaticity parameter γ that allows for a rough classification of the ionisation scenario as a function of the ionisation potential and laser field parameters. For this, one may assume that the electron is bound in an infinitely thin potential well of depth I_p, which corresponds to its ionisation potential. It is distorted by the time-averaged electric field of amplitude E_L, forming a triangular barrier. The resulting tunnel length is $l = I_p/(eE_L)$ and the kinetic energy the electron carries after tunneling equals the ionisation potential. Hence the tunneling frequency ω_t can be estimated via the resulting tunneling period T_t and velocity v_t:

$$\omega_t = \frac{2\pi}{T_t} = \frac{2\pi v_t}{l} = \frac{2\pi e E_L}{\sqrt{I_p m_e/2}} \approx \frac{eE_L}{\sqrt{2I_p m_e}} \tag{2.4}$$

The above expression suggests that the tunneling process only depends on the laser intensity, but once $\omega_t \ll \omega_L$ a tunneling current cannot build up during one laser cycle. In this case, the ionisation becomes laser frequency dependent, hence approaching

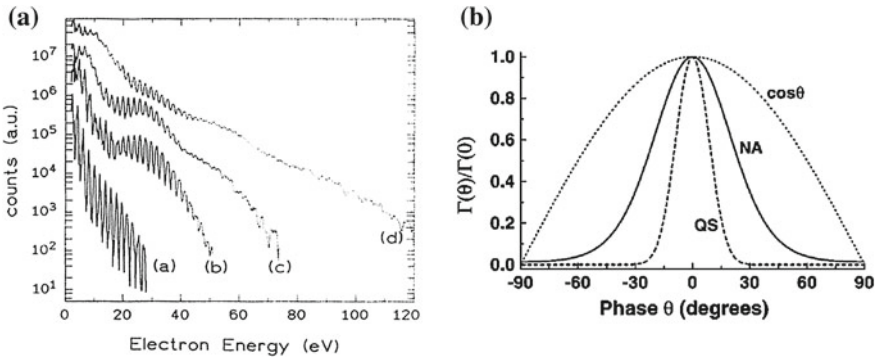

Fig. 2.2 **a** ATI spectra in Ar using 40 fs, 630 nm pulses. The employed intensities are 0.6 (*a*), 1.2 (*b*), 2.4 (*c*) and $4.4 \times 10^{14}\,\mathrm{W\,cm^{-2}}$ (*d*). The *right panel* **b** displays calculated instantaneous ionisation rates $\Gamma^{(TI)}$ in He as a function of the laser field phase. The employed laser parameters are $\lambda = 780\,\mathrm{nm}$ and $I = 5 \times 10^{13}\,\mathrm{W\,cm^{-2}}$. Both quasistatic (*QS*) and nonadiabatic (*NA*) rates are shown, together with the cosine shape of the laser field (Reprinted with permission from [9] and [13]. Copyright (1994) and (2001) by the American Physical Society)

the MPI scenario. The Keldysh parameter is thus defined by comparing tunneling and laser frequency:

$$\gamma = \frac{\omega_L}{\omega_t} = \frac{\omega_L \sqrt{2 I_p m_e}}{e E_L} = \sqrt{\frac{I_p}{2 U_p}} \tag{2.5}$$

such that for $\gamma \ll 1$ TI and for $\gamma \gg 1$ MPI dominates. $\gamma \approx 1$ is an intermediate regime where high order perturbation theory and non-perturbative methods may be appropriate. The tunneling regime is often referred to as the pure strong field regime and will be discussed in more detail in the Sect. 2.1.2. The transition between the regimes can be illustrated via ATI spectra recorded at different intensities as shown in part (a) of Fig. 2.2. Starting from an exponentially decaying spectrum (pure MPI), an additional plateau is formed at higher intensity (intermediate regime). At even higher intensities the peak structure vanishes and multiphoton effects are absent (pure TI).

Even though not included in the Keldysh parameter, strong field ionisation implicitly requires short laser pulses. This is due to the fact that for a longer pulse, the electric field gradient is not steep enough. This means that the increase of the peak field is too slow, such that the ground state population is depleted before the maximum peak intensity of the pulse is reached. In particular for pulses in the visible or NIR spectral range, durations <10 fs are required to access the pure strong field regime [11, 12]. In this context, the saturation intensity I_{sat} is defined as the effective intensity were the ground state population is fully depleted. In this saturation regime, the ionisation rate remains constant with increasing intensity.

2.1.2 Tunneling Ionisation

There is a wealth of theoretical approaches to TI that have entertained theoretical physicists since Keldysh's early work. One branch has developed from extensions to Keldysh's theory [14, 15] into the so-called Strong Field Approximation (SFA) [16]. Based on a semiclassical treatment, Perelomov, Popov and Terent'ev developed another tunneling model (PPT) [17–19] that was further extended by Ammosov, Delone and Krainov and is now known as ADK-theory [20]. Luckily, all tunneling models lead to the same qualitative exponential ionisation rate that is observed experimentally (for a comparison see for example [21]). In atomic units (where the elementary charge, electron mass, reduced Planck's constant and Coulomb's constant are set to unity), the tunneling rate can then be expressed as follows:

$$\Gamma^{(TI)} \propto \exp\left(-\frac{2}{3}\frac{(2I_p)^{3/2}}{E_L}\right) \tag{2.6}$$

For this thesis, SFA is of particular interest as it was developed for also including the free electron's motion in the laser field after TI, which is described in the following Sect. 2.1.3. The SFA comprises a set of approximations, in order to transform the TI event into an analytically solvable problem:

1. *Single Active Electron* (*SAE*) Only one electron is considered in the ionisation event, while the interaction with the remaining electronic states is neglected [12, 22]. Furthermore, only the ground state is taken into account in the evolution of the system. This is reasonable as long as multi-electron excitations are significantly less probable than single-electron excitations, which is usually the case for noble gas atoms and small molecules in NIR fields [12].
2. *Dipole Approximation* (*DA*) The electric field is spatially homogeneous on the scale of the atom, which is treated as an electric dipole. This implies that the laser wavelength is significantly longer than the atomic dimensions, which is justified for NIR radiation and small molecules.
3. *Strong Field Approximation* (*SFA*) The laser field is included exactly and treated classically, while the Coulomb potential acts as a perturbation. The zeroth-order SFA thus completely neglects the potential. Due to the exponential decay of the TI rate with decreasing field strength (see Eq. 2.6), ionisation only takes place efficiently near the peak of the field (see part (a) of Fig. 2.2). In the strong field regime, the laser field is thus much stronger than the Coulomb potential at the moment of ionisation. This is the main justification for the SFA.
4. *Quasistatic Approximation* (*QSA*) The laser field oscillations are slow compared to the atomic response. For this, the electric field is treated as a slowly varying DC field. The frequency dependence of the ionisation rate thus vanishes. Strictly speaking this is only justified in the pure strong field regime, where $\gamma \ll 1$ [13]. However, in the guise of PPT and ADK models, the QSA has been verified experimentally for rare gas atoms [21] and a range of small molecules [23] up to $\gamma \approx 3$. Nevertheless, this is not sufficient if one is interested in sub-lasercycle dynamics

in this intermediate regime. This is the case for measurements involving the CEP of few-cycle pulses, for example. For this, Yudin and Ivanov have developed an extension of the PPT model for calculating sub-cycle, time-dependent ionisation rates independent of the value of γ [13] (see part (b) of Fig. 2.2). The model does not rely on the QSA and is referred to as non-adiabatic tunneling.

Many strong field effects can be understood within the SFA framework. Key findings in the context of this thesis are summarised below.

Properties of the tunneled electron

In the simplest approximation, the electron is assumed to appear in the continuum at position zero with zero momentum. This omits the finite width of the tunneling barrier and initial momentum spread of the tunneled electron. However, as initial conditions for a classical propagation of the free electron in the laser field they reproduce surprisingly many experimental observations (see Sect. 2.1.3). In a more rigorous quantum mechanical treatment there is not a single final continuum state—in this case associated with zero momentum. Rather, during ionisation some population from the electronic ground state is transferred to a set of continuum states, each associated with a particular electron momentum. The free electron is thus described as the superposition of all possible momentum states in the continuum, weighted by their respective transition probability. The resulting wavepacket's transverse velocity distribution is relevant for this thesis and can be expressed in atomic units as follows [24]:

$$\psi(v_\perp) = \psi(0) \exp\Big(- \frac{v_\perp^2}{2} \frac{\sqrt{2I_p}}{E_L} \Big) \tag{2.7}$$

where $\psi(0)$ is the normalisation factor and $|\psi(v_\perp)|^2$ is the probability of the electron to have the transverse velocity $v_\perp$ after tunneling. The distribution is centered at zero transverse momentum, justifying the classical initial conditions. In longitudinal direction, the emerging wavepacket has a more complicated shape. Also, its centre is shifted towards the laser field's acceleration direction [24], with $v_\parallel^2/2 \ll I_p$ in atomic units [13]. However, upon being accelerated further by the laser field, the wavepacket's center of mass motion quickly approaches the trajectory from the above classical treatment [24]. Because of this, the longitudinal velocity distribution is neglected in the remainder of this thesis.

Ellipticity dependence

In this thesis ion yields for different laser pulse ellipticities are compared. Introducing an ellipticity reduces the electric field amplitude, but also changes its time dependence. This has an impact on the average ionisation rate per laser pulse. The TI rate in Eq. 2.6 is presented in the quasistatic limit and is thus time-independent. In an experiment however, the total ion yield from an entire laser pulse is measured. This requires integrating $\Gamma^{(TI)}(E_L(t))$ over the duration of the pulse, which results in different average ionisation rates per pulse depending on its polarisation state. This becomes clear when comparing the electric field amplitude of a linearly and

circularly polarised wave as limiting cases. An arbitrarily polarised electromagnetic wave can be written as:

$$\mathbf{E}(t) = E_x \sin(\omega_L t)\hat{x} + E_y \sin(\omega_L t + \phi)\hat{y} \tag{2.8}$$

Setting $E_x = E_y = E_L$, the wave is linearly polarised for $\phi = 0$ and circularly for $\phi = \pi/2$, such that:

$$|E^{(lin)}(t)| = E_L\sqrt{2}|\sin(\omega_L t)| \tag{2.9}$$

$$|E^{(cir)}(t)| = E_L \tag{2.10}$$

In the long pulse regime, it turns out that the ionisation yield is reduced when changing the laser pulse polarisation from linear to circular. Hence, for obtaining the same ionisation rate, the intensity and thus electric field of the circularly polarised pulse has to be increased. Theoretical calculations of the TI rate lead to $I^{(lin)} = 0.65I^{(cir)}$, as the intensity relationship for achieving this [25]. This has been verified experimentally for atoms and small molecules [25, 26], including CO_2 [27].

Multielectron effects

One particular shortcoming relevant in the context of this experiment is the single active electron (SAE) approximation, which neglects the states of the remaining electrons during the ionisation process. It has therefore been suggested that the rapid removal of an electron through ionisation may lead to non-adiabatic multielectron (NME) dynamics in the ion, resulting in core excitation [28, 29]. Such channels have been observed in atoms [30–32], diatomics [33] and large polyatomics [29] and predicted to be relevant in CO_2 [34]. Their dependence on the laser parameters, however, is not trivial as it involves the coupling of the contributing tunnel-ionisation channels with the time-evolution of the remaining electron states, including the electric dipole field created by the tunneling electron [33]. This will be discussed in more detail in the case of strong field ionisation in molecules (see Sect. 2.3.2).

Over-the-barrier ionisiation (OTBI)

When the laser intensity becomes high enough, the barrier can be suppressed below the ground state. This is illustrated in part (c) of Fig. 2.1. The electron can escape over the barrier without tunneling and the ground state is depleted. For this, the onset of OBTI is associated with ionisation saturation in the pure strong field regime. The corresponding critical intensity can be approximated as [3]:

$$I^{(OTBI)} = \frac{c_0\epsilon_0^3\pi^2 I_p^4}{2Z^2e^6} \tag{2.11}$$

where Z is the charge state of the corresponding atom or ion.

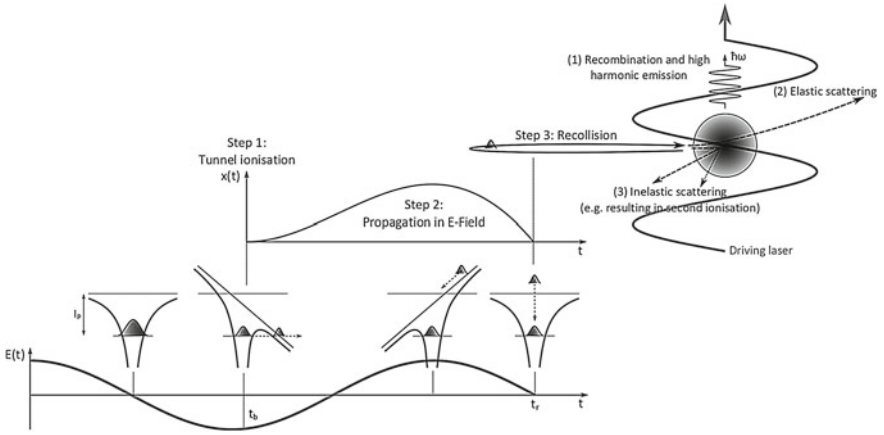

Fig. 2.3 Illustration of the 3-step model as explained in the text. The possible recollision effects are depicted in the inset at the *upper right corner* (Adapted from [38], with permission from Springer Science+Business Media)

2.1.3 Free Electron Dynamics and Recollison

After TI, the electron is rapidly driven away from the ion. However, due to the oscillatory motion of the laser field, the free electron can be driven back to recollide with the parent ion. Upon recollision the electron may recombine to its original ground state or scatter off the ion elastically or inelastically. Recombination results in high harmonic generation (HHG) (see Sect. 2.1.5), elastic scattering in high order ATI [35] and inelastic scattering may lead to further excitation or ionisation of the parent ion (see Sect. 2.1.4). Via this set of effects, laser driven electron recollision has established itself as a versatile tool to probe ultrafast molecular dynamics [36]. The first model for recollision was developed by Corkum [22] and Kulander et al. [37] and is based on a semiclassical treatment and called the 3-step model. It is illustrated in Fig. 2.3. Here, the first step is TI, followed by a classical propagation of the free electron as the second step. The third step is recollision with the possible outcomes mentioned above. However, a fully quantum mechanical treatment based on the SFA was developed soon after by Lewenstein et al. in the context of HHG [16].

Classical free electron propagation

The simplest approach for describing the propagation of the electron wavepacket is to treat its center of mass motion classically. Furthermore the SFA is applied by neglecting the influence of the Coulomb potential during the propagation in the continuum. This is justified as the electron is driven far away from the ion before the laser field approaches a zero crossing of its cycle. Here the electron trajectories are determined using a monochromatic, linearly polarized laser field:

$$\mathbf{E}_L(t) = -\frac{\partial \mathbf{A}(t)}{\partial t} = \mathbf{e}_z E_L \sin(\omega t) \tag{2.12}$$

where $\mathbf{e}_z$ is the unit vector along the z-coordinate axis. Equation (2.12) also defines the *vector potential* $\mathbf{A}$ of the electric field. The classical initial conditions for the tunneled electron have been presented in Sect. 2.1.2. Here they are written as $v(t_b) = 0$ and $z(t_b) = 0$, where t_b denotes the birth time of the electron within the laser cycle and $v = v_{\parallel}$ its longitudinal velocity along the z-axis. The motion of the electron is then determined by Newton's equations of motion, where I mainly follow the derivation of Lein [36]:

$$\ddot{z}(t) = -e/m_e E_L \sin(\omega t) \tag{2.13}$$

$$\dot{z}(t) = v(t) = \frac{eE_L}{m_e\omega}\Big(A(t) - A(t_b)\Big) = \frac{eE_L}{m_e\omega}\Big(\cos(\omega t) - \cos(\omega t_b)\Big) \tag{2.14}$$

$$z(t) = \frac{eE_L}{m_e\omega^2}\Big(\sin(\omega t) - \sin(\omega t_0) - \omega(t - t_b)\cos(\omega t_b)\Big) \tag{2.15}$$

From Eq. (2.14) one can infer that the electron velocity consists of a constant drift term $v_{drift} = -\frac{eE_L}{m_e\omega}\cos(\omega t_b)$ and an oscillating term. The resulting kinetic energy is then given by [36]:

$$E_{kin}(t, t_b) = \frac{1}{2}m_e v^2(t) = 2U_p\Big(\cos^2(\omega t) - 2\cos(\omega t)\cos(\omega t_b) + \cos^2(\omega t_b)\Big) \tag{2.16}$$

Recollision

The condition for recollision in a linearly polarised field is the return of the electron to the vicinity of the parent ion, before it is driven away again in the next laser cycle:

$$z(t_r) \leq \sigma_{ion} \tag{2.17}$$

where σ_{ion} is the recollision cross-section of the parent ion; typically assumed to be on the order of the Bohr radius a_0, such that $\sigma_{ion} \approx a_0^2 \approx 10^{-21}$ m^2, depending on the size of the atom or molecule. Here, t_r is the recollision time with $t_r > t_b$ such that $\tau = t_r - t_b$ is the *return time* of the recolliding electron. Whether recollision takes place or not only depends on the initial conditions and thus birth phase ωt_b of the free electron. Via Eq. 2.16, the recollision energy can then be calculated as $E_r = E_{kin}(t_r, t_b)$. It was first shown by Corkum [22] that the maximum kinetic energy upon recollision can be approximated as:

$$E_r^{(max)} \approx 3.17U_p \propto I\lambda^2 \tag{2.18}$$

corresponding approximately to a birth phase of 17° and a recollision phase of 270° after a peak of the electric field [39]. Note that the recollision energy scales linearly with intensity and quadratically with the laser wavelength. A longer wavelength leads to more time spent in the continuum, allowing the electron to be accelerated for a longer time.

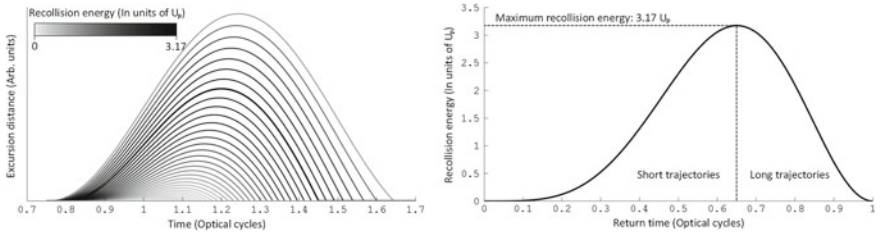

Fig. 2.4 Classical recollision trajectories from the second peak in a sinusoidal laser cycle; calculated via the formulae presented in the text. Both panels illustrate that for each recollision energy there are two types of trajectories: one with a short and one with a longer return time (Reprinted from [38], with permission from Springer Science+Business Media)

A set of trajectories with identical birth phases is launched every half cycle of the laser field, but in opposite directions. However, each trajectory within such a set occurs with a probability given by the TI rate resulting from the associated birth phase within the laser cycle. The exponential decay of the TI rate with the laser electric field thus acts as a narrow filter that confines the contributing birth phases to the peak region of each half cycle. A set of classical trajectories from a sinusoidal laser half-cycle is displayed in Fig. 2.4.

Note that any momentum component perpendicular to the tunneling direction of the electron will drive it away from the remaining ion. This manifests itself in a strong laser polarisation dependence of the recollision step, such that the electron cannot recollide for circular polarisation. In the case of rare gas atoms and small molecules it has in fact been observed experimentally that the electron does not recollide for laser ellipticities larger than $\epsilon \approx 0.3$ [40].

However, there are exceptions to this rule. First, the transverse velocity spread of the electron wavepacket (see Eq. 2.7) may drive the electron away from the ion, reducing the recollision probability. An elliptically polarised laser pulse can then compensate for the initial transverse momentum. This means that recollision may take place at higher ellipticities. In the case of atoms, this effect has thus far only been suggested to be significant in Mg [41]. In the case of molecules, their orbital structure may increase the transverse velocity spread of the tunneled electron. This can then lead to a maximum recollision probability for non-zero ellipticity. This effect is discussed in detail in Chap. 6. Second, when the electron gets close to the parent ion upon its return, it may be attracted by its Coulomb potential. This *Coulomb focussing* effect may compensate for a transverse offset of the recolliding electron in an elliptical driving laser field [42]. Here, it should also be mentioned that the ejected electron may only recollide after several laser cycles (see for example the analysis of [43]).

Direct electrons and elastic scattering

If the electron does not recollide and the laser pulse is longer than a few cycles, the electric field oscillations acting on the electron will vanish adiabatically. Therefore, the kinetic energy and momentum of such a *direct electron* is determined by its drift

velocity and hence birth phase:

$$E_{drift} = 2U_p \cos^2(\omega t_b) \tag{2.19}$$

$$p_{drift} = 2\sqrt{U_p}\cos(\omega t_b) \tag{2.20}$$

Note that the maximum drift energy $E_{drift}^{(max)} = 2U_p$ is acquired at the zero crossing of the electric field (peak of the vector potential). If ionisation takes place at the peak of the electric field (zero crossing of the vector potential), the corresponding drift energy will be zero. The same holds true for the drift momentum. Direct electrons are responsible for the plateau observed in ATI [35]. For completeness it should also be mentioned that if the electron recollides elastically it will gain drift energy in addition to the recollision energy. Numerical calculations based on the classical propagation show that a maximum drift energy of about $10U_p$ can be reached in this case [35]. This energy corresponds to the cut-off in high order ATI spectra in the tunneling regime.

Quantum mechanical picture and further corrections

In the quantum mechanical picture, the response of an atom to a laser field is modeled by the time-dependent Schrödinger equation (TDSE). Employing the single active electron and dipole approximation the TDSE takes the following form in the so-called length gauge (see for example [6]):

$$i\hbar\frac{\partial}{\partial t}\psi(\mathbf{r},t) = \Big[-\frac{\hbar^2\nabla^2}{2m} + V(\mathbf{r}) + \boldsymbol{\mu}\cdot\mathbf{E}_L(t)\Big]\psi(\mathbf{r},t) \tag{2.21}$$

where $V(\mathbf{r})$ is a one-electron potential and $\boldsymbol{\mu}$ the dipole transition operator that describes the electronic response to the laser field $\mathbf{E}_L(t)$. The above TDSE is the starting point for many theoretical treatments including the SFA and of course ab initio calculations. As a more detailed discussion is beyond the scope of this thesis, I will only highlight the most significant modifications of the quantum mechanical picture with respect to the previously discussed classical model that are relevant to this thesis. Here, the recolliding electron is a fraction of the ground state population driven into the continuum. Recollision can then be interpreted as the interaction between the remaining ground state population ψ_g and the returning continuum wavepacket ψ_c. The evolution of the continuum wavepacket is often modeled via the Feynman path integral approach. Here, the phase accumulated by the spatial parts of the wavepacket over time is related to the action S along the classical trajectory presented previously [12, 24]:

$$\psi_c(\mathbf{r},t) \propto \sqrt{\Gamma^{(TI)}(t_b)}\exp\Big[iS(\mathbf{r},t,t_b)\Big] \tag{2.22}$$

where the TI rate determines the initial wavepacket distribution, as discussed earlier. Generally, different spatial parts of the wavepacket correspond to different momenta along the classical trajectory and thus different energies. Within the SFA framework,

the Coulomb potential is neglected for the propagation and the wavefunction of the unperturbed free electron becomes a plane wave, called *Volkov state*. Here, an analytical expression for the action can be obtained [(in atomic units (a.u.)]:

$$S(\mathbf{r}, t, t_b) = [\mathbf{A}(t) - \mathbf{A}(t_b)]\mathbf{r} - \frac{1}{2}\int_{t_b}^{t} [\mathbf{A}(t') - \mathbf{A}(t_b)]\, dt' \tag{2.23}$$

where $\mathbf{v}(t) = \mathbf{A}(t) - \mathbf{A}(t_b)$ is electron's instantaneous kinetic momentum along the classical trajectory.

In this picture, the recollision probability depends on the overlap between the returning continuum wavepacket and the remaining ground state population. Two properties of the electron wavepacket may reduce the probability: wavepacket spreading in the continuum and its transverse velocity spread upon its birth. Wavepacket spreading increases with the time spent in the continuum. This only depends on the driving laser wavelength λ. This effect has been investigated theoretically with HHG as a probe. Here, numerical solutions to the time-dependent Schrödinger equation (TDSE) for the HHG emission of a single atom have shown a reduction of the emission scaling as $\lambda^{-5.5\pm0.5}$ [44].

2.1.4 Nonsequential Double Ionisation

Non-sequential double ionisation describes the double ionisation of an atom or molecule, for which the two ionisation steps are correlated. This is not the case for *sequential double ionisation*, where each ionisation happens independently of the other. NSDI was first observed in form of a knee structure in the ion yields in Xenon as a function of intensity [45, 46]. Along with the recollision model, where the two ionisation steps are separable in time, two instantaneous mechanisms were proposed to explain the effect: *shake-off* [47] and *collective tunneling* [48]. In shake-off, a single high energy photon is absorbed ($\hbar\omega \gg I_p$), such that the ionisation process is so fast that the remaining electrons cannot adiabatically readjust to form the orbital of the ion [49]. The resulting non-adiabatic multi-electron dynamics then cause excitations that lead to further ionisation of the parent ion. In collective tunneling, multiple electrons simultaneously tunnel through the finite barrier. In its first proposal, however, Eichmann already points out that ionisation rates of this mechanism are quantitatively too low to account for laser driven NSDI. Fittinghoff et al. [50] then give a first strong indication for rescattering being the main mechanism, by measuring the polarisation dependence of He^{++} and Ne^{++} yields. In particular a suppression of the knee structure for circular polarisation was observed, which can only be explained in the rescattering model.

Within the recollision model, two NSDI channels are possible (see for example [51]):

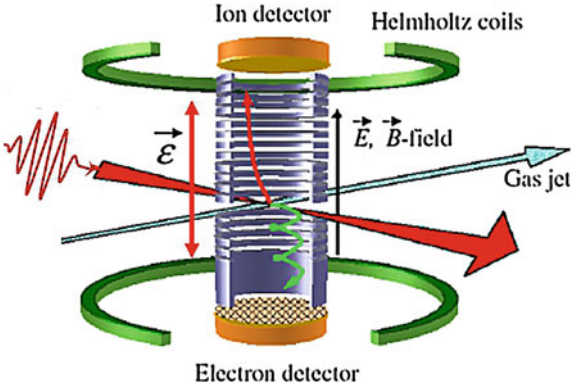

Fig. 2.5 Schematic sketch of the reaction microscope typically used for differential recoil ion measurements. The sample is delivered in form of a rotationally cold supersonic gasjet, perpendicular to the laser propagation direction. Ions and electrons are extracted via electric and magnetic fields respectively and detected in coincidence via position-sensitive micro-channel plate detectors (MCP) in conjunction with delay-line anodes (Reprinted from [51]. ©IOP Publishing and Deutsche Physikalische Gesellschaft. CC BY-NC-SA)

1. *Recollision induced impact ionisation* takes place when the kinetic energy of the recolliding electron is higher than the ionisation potential of the remaining ion I_p^+, such that the second electron is released instantaneously upon recollision. Note that in this case, the recollision phase of the first electron corresponds to the birth phase of the second one. This channel is sometimes denoted as (e, 2e).
2. *Recollision-excitation with subsequent field ionisation* (RESI) was first proposed by Feuerstein et al. [52] and takes place when the kinetic energy of the electron is below I_p^+. In this case the ion is lifted to an excited state upon recollision, such that it can be field-ionised near one of the subsequent peaks of the laser field. Note that there is a time delay between recollision of the first and release of the second electron.

In order to provide clear evidence for the recollision model and a separation of the two possible channels, numerous differential measurements of the recoil ion momentum in NSDI were performed [51–55]. Using a reaction microscope like in *Cold Target Recoil Ion Momentum Spectroscopy* (COLTRIMS, for a review see for example the article by Dörner et al. [56], a simplified setup is illustrated in Fig. 2.5), the recoil momentum vectors of the doubly ionised ion and the two ejected electrons are determined via their position on the detector and time-of-flight (TOF). A kinematic analysis of these vectors is based on momentum conservation during recollision (neglecting photon momenta) and the fact that the two electrons are detected as directed electrons, with drift momenta corresponding to Eq. (2.19). Note that in this case the relevant phase of the recolliding electron is its recollision phase, as this is the point in time when it is eventually driven into the continuum by the laser field. The electron and ion momenta therefore reveal the laser field phase in which the particles were released and therefore enable one to distinguish between the NSDI channels described above. This is illustrated and summarised in Fig. 2.6. Several studies have

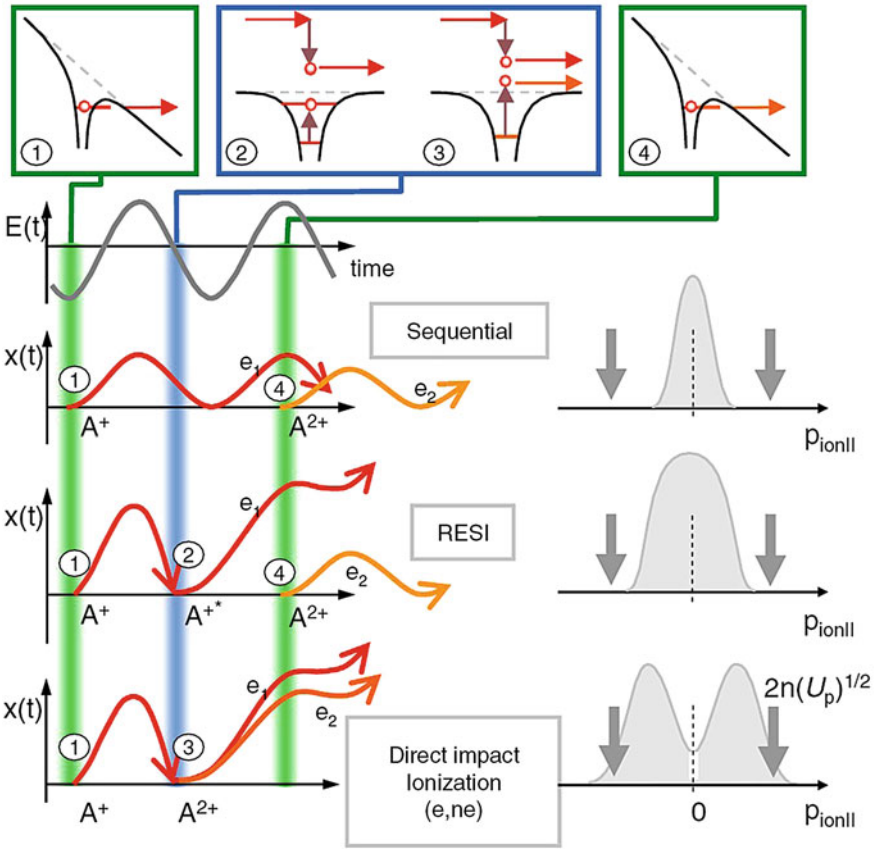

Fig. 2.6 Summary of the possible double ionisation channels (taken from [57]). The first electron is created at (*1*) via tunneling ionisation. In sequential ionisation, the second electron is tunnel ionised after one cycle at the peak of the field (*4*) and hence both electrons have very small momenta. This is shown in the corresponding ion momentum distribution. In RESI, the first electron recollides at (*2*), excites the atom and a second electron is tunnel ionised afterwards at (*4*). This leads to a broader ion momentum distribution around zero due to the excitation energy. In direct impact ionisation, both electrons acquire a large drift momentum, such that the ion momentum distribution has a characteristic dip at zero. The *arrows* point at the maximum drift momenta (Reprinted with permission from [57]. Copyright (2004) by the American Physical Society)

been conducted to determine the dependence on atomic structure and laser pulse parameters of the three double ionisation channels. They are briefly reviewed in the following paragraphs.

Atomic structure

The dependence on the atomic structure can be illustrated by comparing a light atom like Ne to a heavier one like Ar (see for example [51, 58, 59]). For comparable intensities, the RESI channel is much more significant in Ar than in Ne, as shown

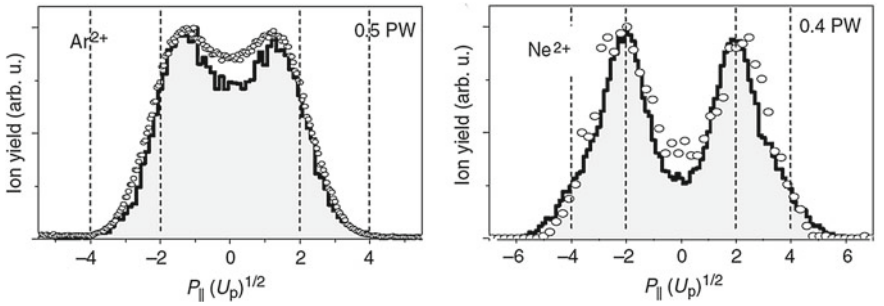

Fig. 2.7 Ion momentum spectra from Ar and Ne at 800 nm (*circles*) and 1300 nm (*solid line*) [51]. The experiment was performed using 30 fs at 800 nm and 35–40 fs at 1300 nm pulses with the intensity denoted in PWcm^{-2} in the figure. The momenta are given in units of $\sqrt{U_p}$ in order to account for the difference in ponderomotive potential (Reprinted from [51]. © IOP Publishing and Deutsche Physikalische Gesellschaft. CC BY-NC-SA)

in Fig. 2.7. By comparing ion momentum spectra with similar ratios of recollision energy to the second ionisation potential $3.17U_p/{I_p}^+$, de Jesus et al. [58] attribute this to the larger excitation cross-section of Ar. Alnaser et al. [59] argue that the scaling of the above recollision energy ratios is limited by the atom's saturation intensity I_{sat}. Therefore the difference in ionisation potentials cannot be excluded at all intensities in this way but the authors argue that it will always manifest itself in the Keldysh adiabaticity parameter $\gamma = \sqrt{I_p/U_p}$. Thus at 800 nm $\gamma^{(Ar)} = 0.6$ and $\gamma^{(Ne)} = 0.4$, such that Ne is further in the tunneling regime and hence favouring the recollision scenario with direct impact ionisation.

Laser pulse parameters

Broad studies have been performed by [55, 59] for example. Starting from a direct impact ionisation scenario, both decreasing and increasing the intensity will lead to a single peak ion momentum distribution [55]. For low intensities the RESI channel will dominate, as the recollision energy drops below ${I_p}^+$ and the first ionisation step will enter the multi-photon regime. For high intensities the sequential ionisation channel will dominate. The wavelength dependence is qualitatively similar to intensity, but quantitatively stronger due to its quadratic scaling in U_p. Several studies [51, 59] show that the impact ionisation channel becomes increasingly dominant for higher wavelengths. This is due to an increase in recollision energy and decrease in the Keldysh parameter and hence going deeper into the tunneling regime. Figure 2.7 shows that for longer wavelengths the dip at zero momentum becomes more pronounced, which corresponds to a stronger impact ionisation channel.

In addition to the above discussion, Liu et al. [60] showed that the carrier envelope phase (CEP) of a few-cycle pulse influences the NSDI ion momentum spectra, by introducing a pronounced asymmetry in the ion ejection direction. The experiment was performed in Ar using 5 fs, 500 μ J pulses at 760 nm. Nevertheless, their numerical simulation showed that this impact vanishes for pulses as long as 8 cycles, which

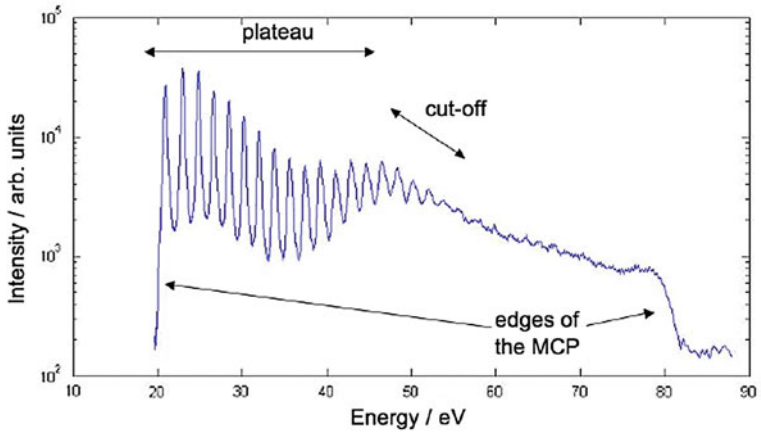

Fig. 2.8 Typical HHG spectrum that displays the essential features described in the text. Here, MCP refers to the multichannel plate detector used to record the spectrum (Figure and measurement courtesy of Thomas Siegel)

corresponds to approximately 21 fs at 800 nm. This effect is thus not relevant in the context of this thesis.

2.1.5 High Harmonic Generation

Upon recollision, the electron may recombine with the parent ion. This is followed by the emission of its recollision energy in form of a single photon, which is an integer multiple of the driving laser photon energy. The process is thus called High Harmonic Generation (HHG). In the quantum mechanical treatment, the recombination of the free electron with the ground state is modeled as rapid oscillations of the resulting orbital wavefunction and hence atomic electron density. The recollision process thus represents a time-dependent induced dipole moment $\mu_h(t)$, which causes the emission of high harmonic radiation with intensity I_h due to its acceleration [12]:

$$I_h(t) \propto |\ddot{\mu}_h(t)|^2 \tag{2.24}$$

High harmonic emission takes place twice every laser cycle. Due to the coherence of the driving laser field, the harmonic emission of the individual half cycles interfere and lead to an HHG spectrum with discrete peaks spaced by twice the driving laser frequency (see Fig. 2.8). In a monoatomic gas the emission obeys inversion symmetry, such that $\mu_h(t + T_L/2) = -\mu_h(t)$. This implies that the harmonic spectrum only consists of odd integer multiples of the driving laser frequency [3].

In the multiphoton regime, the harmonic intensity decreases very quickly with the harmonic order. This can be understood from the MPI rate from (2.1), as it

decreases rapidly with the number of photons involved. For higher intensity, one enters the tunneling regime and the observed harmonic spectra change. After the decrease of harmonic intensities for the first orders, the spectrum shows a plateau in intensity, which is followed by a very quick cut-off. The cut-off is due to the maximal kinetic energy, the electron can acquire in the driving laser field. Therefore, one can extend the cut-off, by either increasing the intensity or the laser wavelength λ. Both approaches have limitations. The intensity cannot be increased infinitely as one will eventually reach the saturation intensity for the ionisation step. For this reason it is often advantageous to use atoms or molecules with a high I_p in order to increase the laser intensity as much as possible. The wavelength seems to be the better option as the ponderomotive energy scales quadratically with it. Yet the higher wavelength also leads to a rapid increase of wavepacket spreading as discussed earlier. These effects have to be balanced in order to generate high harmonics efficiently.

HHG has become a powerful technique for studying molecular dynamics. On the one hand, one can use the emission spectrum itself to investigate the molecular properties of its source. Due to the return time to recollision energy mapping for each trajectory, the HHG spectrum contains information about the parent ion dynamics during the electron's excursion time (see for example [61]). On the other hand the properties of the emission (ultrahort pulse duration, high brightness, good coherence [6]) open up the possibility of using HHG as a laser pulse source for producing pulses with a duration of a few hundred attoseconds [12]. This in turn provides the opportunity do develop pump-probe like experiments for investigating electron dynamics in atoms and molecules on this time scale.

2.2 Molecules

Accurate modelling of molecular dynamics is an ongoing challenge in physics due to the large number of interacting particles. This section aims at presenting the most common approximations for a qualitative understanding of the dynamics studied in this thesis. They will be restricted to the case of diatomics in time-independent fields. Given that CO_2 is a symmetric, linear molecule, this is a reasonable approach. Extensions due to the possible bend of the molecule and its detailed ionisation and dissociation dynamics are discussed in the respective later chapters.

2.2.1 Electronic Structure

On first sight, molecules might not be very different from atoms: it still comes down to solving the time-independent Schrödinger equation (TISE). The solutions are the molecular eigenstates $\Psi_M(\mathbf{r}, \mathbf{R})$, each uniquely associated with an energy eigenvalue E_M. The latter are the energy levels observed in experiments and are thus important for understanding the evolution of the molecular system. The Born-Oppenheimer

approximation (BOA) leads to a rather accessible description by decoupling electronic and nuclear energy within the molecule. In strong field physics however, the electron density profile or *orbital* is relevant for understanding ionisation in the molecular frame of reference. It is connected to the molecular eigenstate within the framework of the molecular orbital theory. The energy level structure and orbital picture really are two sides of the same coin and are conveniently connected via the classification of quantum states in spectroscopic notation.

The Born-Oppenheimer approximation

The general molecular Hamiltonian can be written in the following form (see for example [62, 63]):

$$H_M = \underbrace{\sum_i -\frac{\hbar^2\nabla_{e,i}^2}{2m}}_{\text{electron kinetic energy}} + \underbrace{\sum_{j>i}\frac{e^2}{|\mathbf{r}_i-\mathbf{r}_j|}}_{\text{electron-electron repulsions}} + \underbrace{\sum_i -\frac{\hbar^2\nabla_{N,i}^2}{2M_i}}_{\text{nuclear kinetic energy}} + \underbrace{\sum_{j>i}\frac{Z_iZ_je^2}{|\mathbf{R}_i-\mathbf{R}_j|}}_{\text{nuclear-nuclear repulsions}}$$
$$+ \underbrace{\sum_{ij} -\frac{Z_je^2}{|\mathbf{r}_i-\mathbf{R}_j|}}_{\text{electron-nuclear attractions}} \equiv T_e + V_e + T_N + V_N + V_{e,N} \tag{2.25}$$

where the $\{\mathbf{r}, \nabla_e\}$ refer to the coordinates and momenta of the electrons and $\{\mathbf{R}, \nabla_N\}$ to the corresponding properties of the nuclei. Z_i denotes the nuclear charge of nucleus i. Apart from the electronic configuration, a molecule has additional degrees of freedom and thus associated energy levels, because of the relative motion of the nuclei. These are vibrations along the molecular axis and rotations around the molecule's center of mass. The BOA now assumes that the electronic configuration can be decoupled from the nuclear motion. This is justified by the large difference between electronic and nuclear mass, such that the electrons move much faster than the nuclei. Therefore, the nuclear geometry is described as a quasistatic framework for the electrons. Their wavefunction then depends only parametrically on the nuclear coordinates $\{\mathbf{R}\}$. The molecular wavefunction can then be separated into an electronic $\psi_e(\mathbf{r}, \mathbf{R})$ and a nuclear part $\psi_N(\mathbf{R})$:

$$\Psi_M(\mathbf{r}, \mathbf{R}) = \psi_e(\mathbf{r}, \mathbf{R})\psi_N(\mathbf{R}) \tag{2.26}$$

This implies that electronic, vibrational and rotational contributions to the molecular energy level structure can also be separated [64]:

$$E_M = E_e + E_{vib} + E_{rot} \tag{2.27}$$

With the internuclear geometry fixed, the electronic wavefunction must fulfill the time independent Schrödinger equation (TISE):

$$H_e\psi_e(\mathbf{r}, \mathbf{R}) = (T_e + V_e + V_{e,N})\psi_e(\mathbf{r}, \mathbf{R}) = E_e(\mathbf{R})\psi_e(\mathbf{r}, \mathbf{R}) \tag{2.28}$$

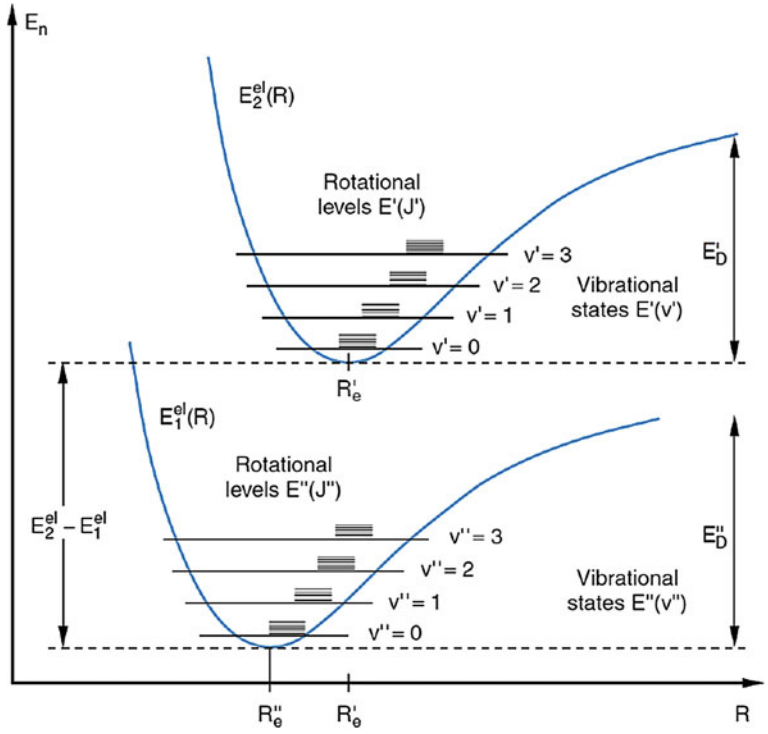

Fig. 2.9 Schematic representation of the rovibrational energy level structure of two electronic states of a diatomic molecule. Here, R_e denotes the equilibrium bond length and E_D the dissociation energy (Reprinted from [65], with permission from Springer Science+Business Media)

Plugging (2.26) and (2.28) into the TISE for the molecular Hamiltonian and neglecting the change of the electronic wavefunction with respect to the nuclear coordinates, one obtains [62, 64]:

$$H_M \psi_N(\mathbf{R}) = (T_N + E_e(\mathbf{R}) + V_N(\mathbf{R}))\psi_N(\mathbf{R}) = E_M \psi_N(\mathbf{R}) \tag{2.29}$$

The molecular energy eigenstate E_M was thus obtained from the nuclear motion in an effective potential consisting of the fast and thus averaged electron-electron and electron-nuclear interaction contained in $E_e(\mathbf{R})$ and the instantaneous internuclear interaction contained in $V_N(\mathbf{R})$. This effective potential can be calculated for every internuclear geometry by solving the electronic TISE (2.28) and including $V_N(\mathbf{R})$, hence giving the potential energy surface (PES) on which the nuclei move [63]. The energy level structure associated with the nuclear part is contained in the molecular energy eigenvalue via Eq. 2.27. In the BOA framework it is thus a fine structure superimposed onto the PES associated with the electronic energy. This is illustrated

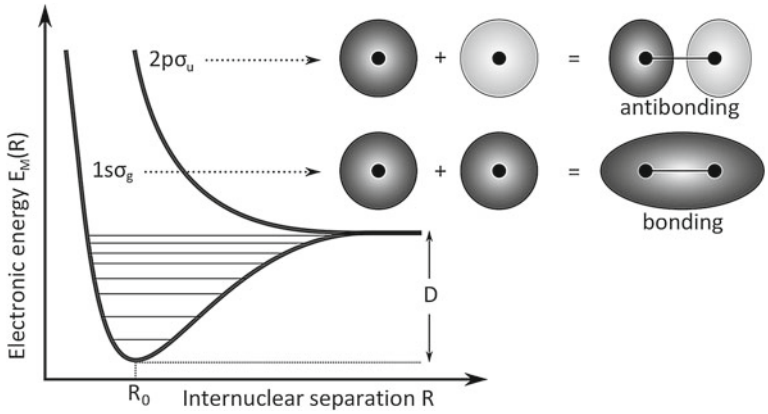

Fig. 2.10 Schematic representation of the PECs corresponding to the bonding and antibonding state of H_2^+ including a graphical representation of the associated linear combination of atomic orbitals as explained in the text. Here, the different shadings of the orbitals correspond to different signs of the electronic wave function

in Fig. 2.9. Note that for a diatomic molecule, the PES is reduced to a potential energy curve (PEC).

Molecular orbital theory

The PECs obtained within the BOA framework illustrate the requirement for chemical bond formation. A local minimum means that the potential energy of the nuclei is lowest for an associated equilibrium bond length R_0. The energy D that is required to overcome the potential well, such that $R \to \infty$, is called the *dissociation energy* or *limit* of this bound state. This is illustrated in Fig. 2.10. Note that this energy is slightly larger than the real chemical dissociation energy, as the vibrational ground state of the molecule is not taken into account [66]. A molecular orbital is proportional to the electronic probability density $|\psi_e(\mathbf{r}, \mathbf{R})|^2$ within the nuclear framework. The molecular orbital corresponding to a bound state typically has a non-zero probability density between the atoms. In principle a calculation of the bound states and their orbitals via the BOA would suffice for a complete description of a molecule. However, exact solutions can only be obtained for the simplest possible molecule H_2^+. In order to simplify the calculations for more complex systems, one may assume that only the electrons on the outer shells contribute to the bond formation, whereas the ones close to the nucleus remain unperturbed [67]. This implies that for distances close to one of the nuclei, the molecular orbital converges to the corresponding atomic one. As the TISE is linear, this suggests that molecular orbitals may be approximated as linear combinations of atomic orbitals (LCAO).

Formally, one would assume that the atomic wavefunctions $\{\psi_{A,i}\}$ form a basis of the molecular Hamiltonian and then take their linear combination as the trial solution for the molecular wavefunction [68]:

$$\Psi_{LCAO} = \sum_i c_i \psi_{A,i} \tag{2.30}$$

For the hydrogen molecular ion, this results in the wavefunctions $\Psi_{LCAO,+} = \psi_{H,1} + \psi_{H,2}$ and $\Psi_{LCAO,-} = \psi_{H,1} - \psi_{H,2}$. They are shown graphically as an inset in part (a) of Fig. 2.10. One observes that for the symmetric linear combination, the resulting wavefunction has a non-zero probability density between the nuclei and is thus called a *bonding* orbital. For the anti-symmetric combination, the density drops to zero there and an *antibonding* orbital is formed. This is directly reflected in the associated PECs, corresponding to a bound and repulsive state, respectively.

Classification of quantum states

As was mentioned previously, every electronic energy eigenstate is associated with a molecular orbital. Each orbital can be uniquely classified by its symmetry properties, which is widely used in spectroscopy to label the energy levels. For diatomics, the three symmetry properties are: rotational symmetry around the molecular axis, inversion symmetry with respect to the molecular centre and reflection symmetry at a plane containing the molecular axis. Formally, the mathematical operators that perform these transformations leave the molecular Hamiltonian invariant and commute, such that they span a complete set of simultaneous eigenfunctions of the molecular system. This means that their quantum numbers uniquely identify each possible electronic energy level [68].

The rotational symmetry is associated with the conservation of the molecule's angular momentum component L_z along the molecular axis z. The corresponding eigenvalue equation with the quantum number Λ is given by [69]:

$$L_z \psi_e = \pm \Lambda \hbar \psi_e, \quad \Lambda = 0, 1, 2, \ldots \tag{2.31}$$

The labeling of the states is done with greek letters as in atoms, such that $\Lambda = 0, 1, 2, \cdots \leftrightarrow \Sigma, \Pi, \Delta, \ldots$. Inversion symmetry is associated with the notion of *parity* of the electronic wavefunction. If the sign of the wavefunction changes (does not change) upon inversion its parity is odd (even). In spectroscopic notation the subscript u (g) is used. For reflection symmetry a change in sign is denoted by a '$-$' superscript. Invariance under reflection is then denoted by a '$+$' superscript. In orbitals with $\Lambda > 0$, this concept is meaningless due to the broken cylindrical symmetry of the wavefunction. This classification is therefore only relevant for Σ states. Note that for atomic orbitals the analogue notation in lower-case greek letters is used for the projection of the angular momentum quantum number. This notation is often used when referring to single electron states within a molecular system [69].

Lastly, a particular quantum state may be degenerate due to the spin of its unpaired electrons. If all electrons are paired, the state is 1-fold degenerate (a singlet). If there is one unpaired electron it can have spin up or down, so the state is 2-fold degenerate (doublet), whereas two unpaired electrons result in a triplet state. This is denoted as the multiplicity $2S + 1$ via the total spin S of the molecular eigenstate. The full term symbol of the state is now written as ${}^{2S+1}\Lambda^{+/-}_{g/u}$. In addition to the term symbol,

energy levels in a molecule are usually ordered according to their excitation energy, starting with the ground state: X, A, B, C, etc.

2.2.2 Radiative Transitions

When a molecule is placed in a laser field, its charge distribution interacts with the laser electric field. Here, the molecule may absorb energy and undergo a transition from its initial energy state Ψ_i to a final state Ψ_f. Within the dipole approximation (see Sect. 2.1.2) the corresponding light-molecule interaction can be treated as a dipole transition (higher multipole interactions are neglected). Neglecting the rotational energy and using the BOA, the state can be separated into electronic ψ and vibrational contributions ν, such that $\Psi = \psi\nu$. Here I have dropped the dependence on the electronic and nuclear coordinates for convenience. Analogously, the transition dipole moment $\boldsymbol{\mu}$ between the states consists of an electronic and a nuclear part with $\boldsymbol{\mu} = \boldsymbol{\mu}_e + \boldsymbol{\mu}_N$. In this way, the transition probability $M_{i\to j}$ can be obtained [69]:

$$\langle \Psi_f | \boldsymbol{\mu} | \Psi_i \rangle = \langle \psi_f \nu_f | \boldsymbol{\mu}_e + \boldsymbol{\mu}_N | \psi_i \nu_i \rangle \tag{2.32}$$

$$= \langle \psi_f | \psi_i \rangle \langle \nu_f | \boldsymbol{\mu}_N | \nu_i \rangle + \langle \nu_f | \nu_i \rangle \langle \psi_f | \boldsymbol{\mu}_e | \psi_i \rangle \tag{2.33}$$

If an electronic transition takes place, $\psi_i \neq \psi_f$ and due to their orthogonality $\langle \psi_f | \psi_i \rangle = 0$. Therefore, the transition probability turns out to be:

$$M_{i\to f} \propto |\langle \Psi_f | \boldsymbol{\mu} | \Psi_i \rangle|^2 \tag{2.34}$$

$$\propto |\langle \nu_f | \nu_i \rangle|^2 \times |\langle \psi_f | \boldsymbol{\mu}_e | \psi_i \rangle|^2 \tag{2.35}$$

The interpretation of the above equation is that the transition probability depends on the dipole transition probability between the two electronic states and on the overlap between initial and final vibrational states.

Electronic transitions

A dipole transition is *allowed* if $\langle \psi_f | \boldsymbol{\mu}_e | \psi_i \rangle \neq 0$. This is only possible if the total integrand of the corresponding integral does not have an odd parity [64]. The parity of the dipole transition operator $\boldsymbol{\mu}_e = -e\mathbf{r}$ is odd, because it has a direction. Therefore only transitions between states of opposite parity are allowed.

Depending on the direction of the transition dipole with respect to the molecular axis, the associated angular momentum Λ may be changed. Direct inspection of the integrand for dipole moments along and perpendicular to the molecular axis leads to allowed transitions for $\Delta\Lambda = 0$ and $\Delta\Lambda = \pm 1$, respectively [64]. This has an important consequence for transitions induced via linearly polarised light in the molecular frame. As the direction of the transition dipole moment is given by the laser field polarisation, this means that only the field component parallel to the molecular axis contributes to transitions with $\Delta\Lambda = 0$. The same reasoning applies

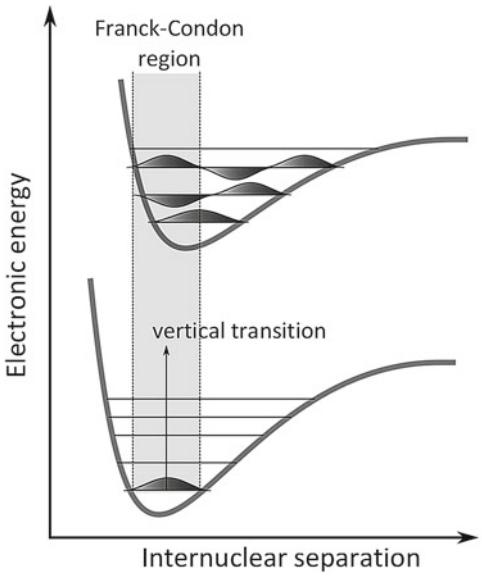

Fig. 2.11 Illustration of the Franck-Condon principle. Assuming that the transition takes place instantaneously, the initial vibrational wavepacket is projected vertically upwards. The transition probability to the final vibrational states scales with their overlap with the projection

to the perpendicular case. This implies the following polarisation dependences for transitions between $\Sigma \rightarrow \Sigma$ ($\Delta\Lambda = 0$) and $\Sigma \rightarrow \Pi$ ($\Delta\Lambda = \pm 1$) states:

$$M_{\Sigma\rightarrow\Sigma} \propto |\cos(\theta)|^2 \tag{2.36}$$

$$M_{\Sigma\rightarrow\Pi} \propto |\sin(\theta)|^2 \tag{2.37}$$

where θ is the angle between the polarisation direction and the molecular axis. As the transition dipole moment operator does not change the total spin S or the reflection symmetry in a parallel transition, the selection rules $\Delta S = 0$ (neglecting spin-orbit coupling) and $\Sigma^{\pm} \rightarrow \Sigma^{\pm}$ hold in addition to the above [64].

Vibrational transitions

By using the BOA it is implicitly assumed that the transition takes place in a quasi-static nuclear framework. This means that the transition is instantaneous without a change in the internuclear distance R. In the context of vibrational transitions, this approximation is called the *Franck-Condon principle* [70, 71]. As derived above, the transition probability to a vibrational state during an electronic transition is given by the overlap between the vertically projected initial vibrational state onto the possible final state. This is illustrated in Fig. 2.11. It is thus called a *vertical* transition, where the corresponding projection region is called the *Franck-Condon region*. The overlap integral $|\langle\nu_f|\nu_i\rangle|^2$ is called the *Franck-Condon factor*.

2.2.3 Field-Dressed States

In the Sect. 2.2.2, the energy level structure and related transitions have been treated perturbatively, meaning that the laser field does not couple to the molecular states. However, in the strong field regime this is not sufficient and the PECs can be significantly altered due to the presence of the field. For a non-perturbative approach, one would work with the time-dependent Schrödinger equation (TDSE) and include the laser field and its interaction with the molecule exactly. The total Hamiltonian of this system would thus consist of the time-independent field free molecular part H_M, the laser field in the quasistatic approximation H_L and the time-dependent interaction with the laser field $E_L(t)$ within the dipole approximation [69]:

$$H_{tot}(t) = H_M + H_L + \boldsymbol{\mu} \cdot \mathbf{E}_L(t) \tag{2.38}$$

A long laser pulse (>10 fs at 800 nm) may be assumed to consist of many identical cycles. Thus the dipole interaction with the molecule will also be approximately periodic with the laser frequency. As in the context of HHG (see Sect. 2.1.5), a periodically driven process in time is related to a spectrum of harmonics of the driving field via Fourier transformation [72]. In the energy domain, this corresponds to an infinite set of coherent states spaced by the photon energy $\hbar\omega_L$ of the laser field. This is the essence of the so-called *Floquet* theorem that thus leads to periodic eigenfunctions $\{\Psi_{tot,i}\}$ with infinite sets of eigenenergies $\{E_{tot,i}\} \pm n\hbar\omega$, where $n = 0, 1, 2, \ldots$ (for more details see for example [72]). The physical interpretation of this solution is that the field free states are *dressed* by the photons of the laser field. In an experiment involving intensities around 10^{14} W cm^{-2}, the number of absorbed photons is very high such that $n = N \pm m$ with $m = 0, 1, 2, \ldots$ and N on the order of 10^{10} [72]. The resulting sets of parallel photon-dressed PECs may cross at a certain internuclear distance, as is shown in Fig. 2.12. Here, the two states have exactly the same energy due to the photon dressing. At this internuclear distance the states are thus resonant by the difference of the dressed number of photons. When this coupling between the states is neglected, the curves cross and are called *diabatic*. The diabatic curves have the shape of the field-free unperturbed curves. However at a resonant crossing, the radiative coupling via the laser field mixes the states—an effect that increases with the laser intensity and decreases with the order of the coupling [72]. The mixed states must appear as off-diagonal terms in the total Hamiltonian. For obtaining the perturbed PECs, the Hamiltonian thus needs to be diagonalised. These coupled PECs are called *adiabatic* curves and do not cross anymore. Instead, a gap opens with a width that increases with the coupling strength [72].

Even though based on a number of approximations, the adiabitic PECs of field-dressed states offer a rather intuitive picture for understanding a number of dissociation mechanisms, as will be shown briefly in the following Sect. 2.2.4.

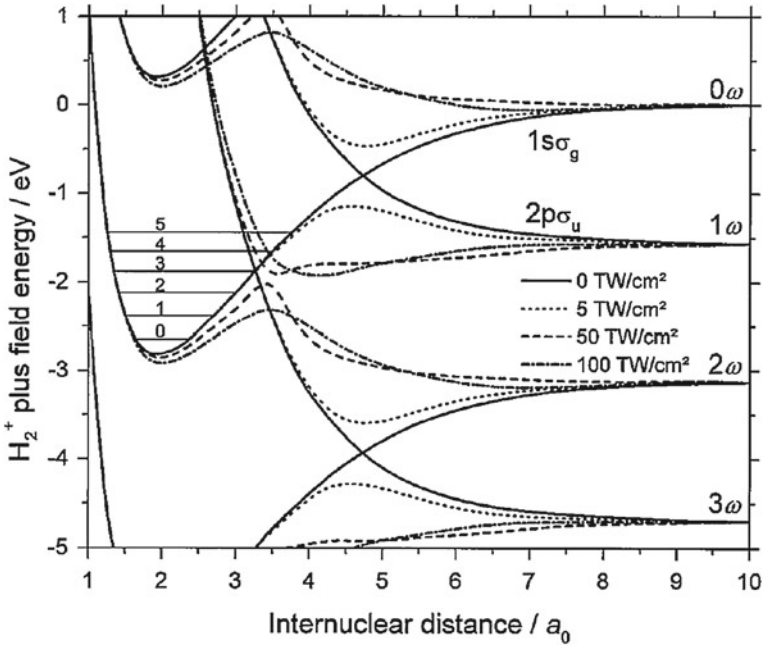

Fig. 2.12 PECs of H_2^+ dressed by a 790 nm laser field. When the field is off, the diabatic representation is appropriate and the *curves* cross (*solid line*). With increasing field strength, avoided crossings are formed at the resonance positions and the resonance gaps become visible in the adiabatic representation (Reprinted with permission from [73]. Copyright (1999) by the American Physical Society)

2.2.4 Dissociation Mechanisms

There are several purely laser induced pathways that may lead to the dissociation of a molecule. On the one hand, the laser field may induce transitions to dissociative states or vibrational states above the dissociation limit. On the other hand, the PECs can be dressed and deformed in such a way that dissociation is either assisted, reduced or delayed in time.

Field-free system

Part (a) of Fig. 2.13 shows the three possible pathways for light induced dissociation in the perturbative regime. (1) shows an electronic transition to a repulsive state. Due to the Coulombic repulsion, these curves are very steep for small internuclear distances, especially in the case of molecular ions with a high charge state. The dissociation products or fragments can thus acquire large kinetic energies E_{kin} as is illustrated in the figure. This dissociation mechanism is called *Coulomb explosion* and is described in more detail below. (2) depicts an electronic transition to an unbound vibrational state, as it lies above the dissociation limit. (3) illustrates a

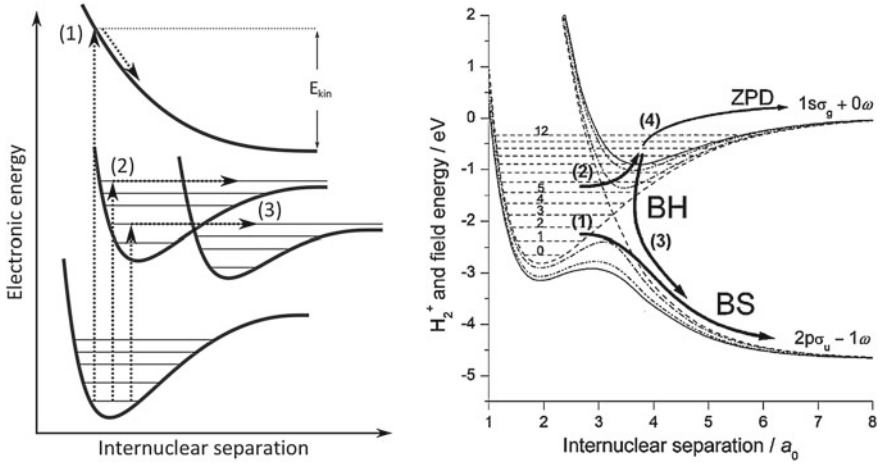

Fig. 2.13 **a** Dissociation pathways in a field free system: transition to a repulsive state (*1*), transition to an unbound state above the dissociation limit (*2*) and predissociation (*3*). **b** Dissociation pathways in a field-dressed system. The figure illustrates the possible dynamics at the 1-photon resonance in H_2^+, dressed by 266 nm photons and a maximum intensity of 5×10^{13} W cm^{-2} (*solid line*, largest gap). Details can be found in text (Part **b** reprinted with permission from [74]. Copyright (2001) by the American Physical Society)

process called *predissociation*. Here, a transition to a bound excited state takes place initially. However, if this excited state is coupled to a dissociative state on another PEC, the molecule may still fragment. Such couplings can internally be established via spin-orbit effects and conical intersections between PECs or externally by collsions for example [66]. Note that in pathways (2) and (3), the excess energy above the relevant dissociation limit is usually on the order of the vibrational level spacing and thus very small compared to (1). The corresponding fragments can typically assumed to be released with a thermal energy distribution centred at zero kinetic energy.

Field-dressed system

Dissociation mechanisms in a field-dressed system can be understood by following the movement of vibrational state distributions along the diabatic and adiabatic PECs. This has been studied intensively in the case of H_2^+ (for reviews see [69, 72]). The most prominent processes are *bond-softening* (BS), *bond-hardening* (BH) and *zero-photon dissociation* (ZPD). They are illustrated in part (b) of Fig. 2.13 in the case of the 1-photon crossing of the bonding $1s\sigma_g$ and the antibonding $2p\sigma_u - 1\omega$ state. At the leading edge of the laser pulse, the intensity is very low and the radiative coupling can be neglected. Here, the diabatic PECs apply (dashed line). When the laser intensity is increased, the 1-photon gap opens at the resonant internuclear distance (the highest intensity corresponds to the solid line). The gap reduces the bound state to a shallow potential barrier. Population in vibrational states higher than this barrier can thus

escape via pathway (1) which corresponds to BS. This process was first observed experimentally by Bucksbaum et al. [75].

At the same time however, the anti-bonding PEC turns into a bound state, due to the potential minimum formed by the 1-photon gap. This means that population in vibrational states above this minimum can be trapped, which is denoted by pathway (2). From here, two different dissociation pathways are possible. Pathway (3) denotes the first, BH, which was first predicted by Giusti-Zusor and Mies [76] and confirmed experimentally only 7 years later by Frasinski et al. [73]. Here, the trapped vibrational population dissociates at the falling edge of the laser pulse, when the gap reduces and the potential minimum turns into a repulsive curve again. Note that the energy of the system is reduced by one photon during this transition. This excess energy is shared by the two fragments in form of kinetic energy. Pathway (4) shows the second dissociation pathway for the trapped vibrational population via ZPD [74]. If the laser intensity increases even further than shown in the figure, the gap becomes larger and flattens out the upper potential minimum and the trapped population becomes unbound. As the population remains on the $1s\sigma_g$ curve throughout this dissociation pathway no photon absorption or emission is involved, hence the name ZPD.

Coulomb explosion

If the electrons of the molecule are stripped off instantaneously with respect to the period of nuclear motion, the internuclear geometry is preserved during this process. The resulting Coulomb repulsion between the remaining nuclii is then given by:

$$\mathbf{F} = \frac{1}{4\pi\epsilon_0} \sum_i -\frac{ZZ_i e^2}{|\mathbf{R} - \mathbf{R}_i|^3} (\mathbf{R} - \mathbf{R}_i) \tag{2.39}$$

Therefore, if one measures the momentum vector of each ejected fragment after the Coulomb explosion, one may use the above equation to reconstruct their initial positions and hence the internuclear geometry, alignment and orientation of the molecule at the instant of explosion [77]. This can be achieved by employing laser pulses with durations significantly shorter than the vibrational period of the molecule in question and intensities generally $>10^{14}\,\mathrm{W\,cm^{-2}}$ [77, 78]. In the PEC picture, this process corresponds to a vertical transition to a repulsive- or Coulombic-curve.

In this process, the pulse duration is the main critical factor for preserving the internuclear structure during the ionisation process. I_2 for example has a vibrational period of roughly 150 fs and hence a 20 fs laser pulse can be used for Coulomb explosion [77]. Furthermore high laser intensities should be employed in order to reach very high charge states. This increases the Coulombic repulsion between the fragments and thus accelerates the explosion process. However, non-adiabatic or post-ionisation alignment may take place in a highly intense laser pulse, which will be discussed in Sect. 2.4.2. While these effects may partially be minimised in the analysis of the fragment momenta, they may be fully suppressed by using circularly polarised light. In this case there is no preferred polarisation direction and the molecules remain randomly aligned in the polarisation plane.

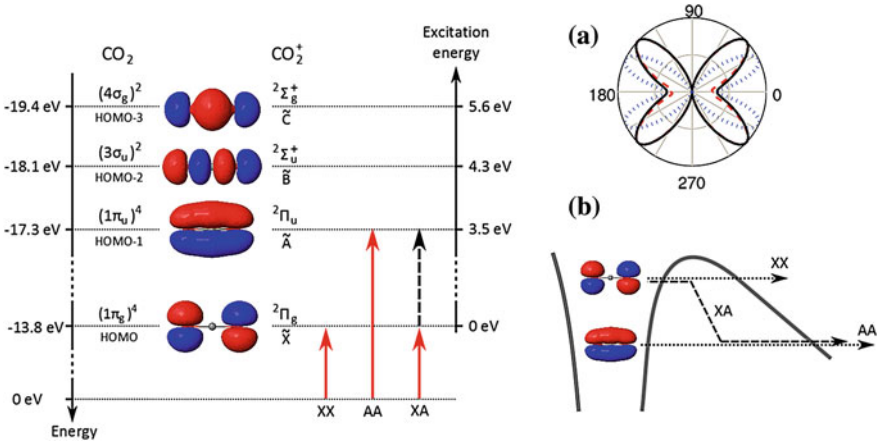

Fig. 2.14 The four highest occupied orbitals in CO_2 and the associated excited ionic states. Three ionisation channels are shown: direct tunneling from HOMO resulting in the ionic ground state (*XX*), tunneling from HOMO-1 (*AA*) and inelastic tunneling from HOMO correlating with HOMO-1. Inset **a** shows the MO-ADK rate from the HOMO (*dotted line*) compared to ab initio solutions of the TDSE using the single active electron approximation and 800 nm laser pulses. The *dashed* and *solid lines* correspond to intensities of 5.6×10^{13} W cm^{-2} and 1.1×10^{14} W cm^{-2}, respectively. **b** Illustrates the three ionisation channels in the inelastic tunneling picture (Part **a** reprinted with permission from [79]. Copyright (2009) by the American Physical Society)

Dissociation in the strong field regime

In the strong field regime, transitions to dissociative states may also take place through tunnel ionisation and inelastic recollisions. This is discussed in more detail in Sects. 2.3.2 and 2.5.

2.3 Molecular Tunneling Ionisation

Due to their non-spherical electronic orbitals and nuclear degrees of freedom, molecular ionisation has additional features compared to atomic ionisation. The most important ones are reviewed in this section with a particular emphasis on CO_2.

2.3.1 Orbital Structure Effects

The rich nuclear structure of molecules leads to orbitals with different symmetry properties, as was discussed in Sect. 2.2.1. One may thus expect that the TI rate in the molecular frame is anisotropic. This is taken into account in the molecular Ammosov-Delone-Krainov (MO-ADK) theory [80] . In this framework, the essential features of the angular ionisation rate are obtained under the assumption that the ionisation

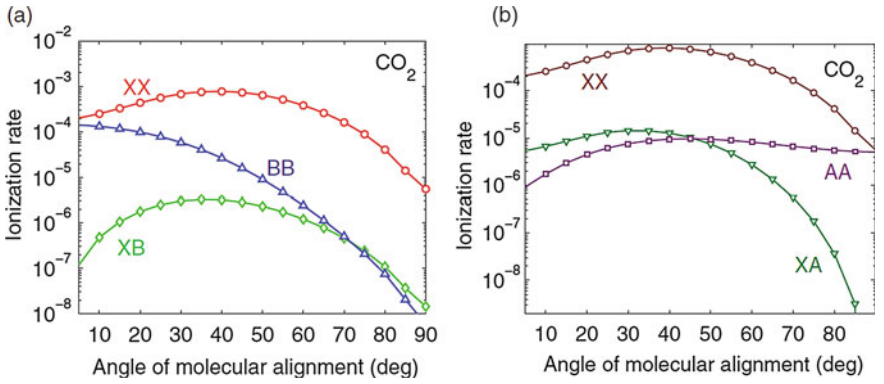

Fig. 2.15 Calculated relative angular ionisation rates for the available channels in CO_2 involving the highest three orbitals. The employed laser pulse parameters are $\lambda = 800\,\text{nm}$ and $I = 0.8 \times 10^{14}\,\text{W cm}^{-2}$. The calculations include the direct channels *XX*, *AA* and *BB* and the inelastic tunneling channels correlating with HOMO; *XA* and *XB* (Reprinted with permission from [89]. Copyright (2012) by the American Physical Society)

probability scales with the electronic density profile of the respective molecular orbital along the ionising laser polarisation direction. This scenario is complicated further by the fact that the occupied orbitals in a molecule typically have different symmetries (see Fig. 2.14). In an experiment, one would observe the superposition of the angular TI rates from all orbitals. However, due to the exponential decay of the TI rate with the ionisation potential I_p, ionisation from the highest occupied molecular orbital (HOMO) is expected to dominate. Yet, it has been observed that the influence of lower lying orbitals cannot be excluded a priori [81–84] - especially not in CO_2. Taking these additional TI channels into account is sometimes referred to as *multichannel strong field ionisation* [84]. Angular ionisation rates for CO_2 from its three highest orbitals obtained in such a framework are displayed in Fig. 2.15.

It should also be added, that experimental ionisation studies in aligned CO_2 show quantitative discrepancies with the MO-ADK model (see inset (a) in Fig. 2.14) [85], suggesting significant shortcomings (alternative approaches and modifications can be found in [79, 86–89] for example). For a qualitative understanding of the experimental results in this thesis however, it is a reasonable tool.

Typically, molecules have decreasing I_p with increasing size. This is associated with the intuitive picture of the outermost electron being further away from the positively charged nuclear framework and thus more loosely bound. However, it was found that most organic molecules have a higher saturation intensity I_{sat} than predicted by their TI rate [90, 91]. Several sources may contribute to this apparent resistance to strong field ionisation. The reduction of the TI rate due to nodal planes in the molecular orbital has already been introduced and is probably the most prominent cause.

2.3.2 Tunneling Excitation

Through TI, the molecular ion may end up in an excited state. Here, two pathways are possible: TI from lower lying orbitals and inelastic tunneling. Both channels may thus lead to the dissociation of the molecular ion.

TI from lower lying orbitals

Previously, TI was presented as the removal of an electron from a given orbital. In the single active electron approximation, the evolution of the remaining electrons is neglected. This is implicit in Koopmans' theorem that says that the remaining electrons do not adjust their distribution during ionisation [92]. This implies that excited states in the parent ion can be reached through ionisation from lower lying orbitals (see Fig. 2.14). Furthermore the ionic state has the same orbital symmetry as its associated state in the neutral. In the molecular frame, the probability of reaching an excited state via this channel thus scales like the MO-ADK rate for the associated neutral orbital. The relative strength of this channel can thus be controlled by the laser polarisation with respect to the molecular axis.

Inelastic tunneling

The breakdown of the SAE has already been mentioned in Sect. 2.1.2. When allowing for nonadiabatic electron dynamics during TI, the different channels may interact. This leads to excitation and deexcitation of the ion and is associated with the electron hole moving to another orbital during TI [89]. This mechanism is thus sometimes referred to as *inelastic tunneling*. It is illustrated for the XA channel in inset (b) in Fig. 2.14. Here, TI from HOMO takes place initially. During tunneling, the hole moves to HOMO-1 leaving the ion in the first excited state A. In this way, the correlation channel does not possess the full exponential suppression of the direct channel (TI from HOMO-1, AA). It has therefore been suggested that inelastic tunneling becomes most relevant for low lying orbitals and low intensity laser fields. Torlina et al. [89] have recently calculated the angular dependence of such correlated channels in CO_2. The results are displayed in Fig. 2.15. It should be pointed out, however, that experimental evidence concerning inelastic tunneling is currently not available.

2.4 NSDI in Small Molecules

As in atomic NSDI, the recollision model also applies to NSDI in small molecules. Similar to the above descriptions, characteristic ion yield enhancements ('knee structures') [93], polarisation dependence [93, 94] and electron-electron correlations in ion momentum spectra from COLTRIMS studies [39, 51, 95] have also been reported in small molecules like H_2, D_2, N_2, O_2 and CO_2. Therefore the overall role of the laser parameters discussed in the Sect. mol:ionmol:exc also holds true for small molecules.

The work by Guo and coworkers [93, 96, 97] serves as a useful reference for the intensity regime in which NSDI in N_2, O_2 and CO_2 can be observed and the

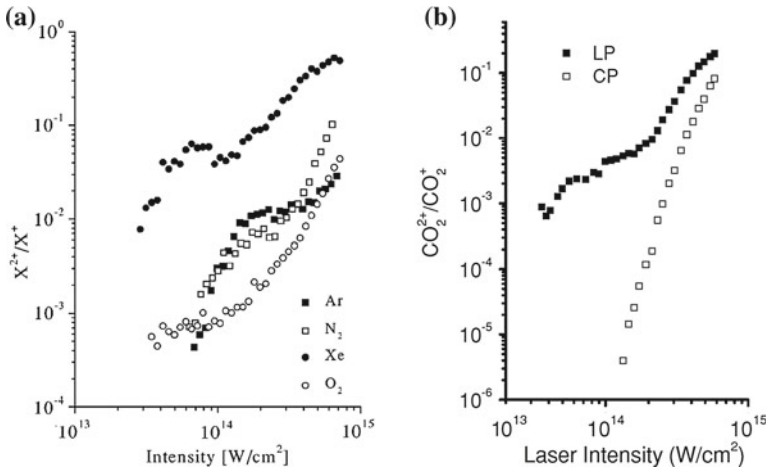

Fig. 2.16 Part **a** displays the X^{2+}/X^{+} ratio explained in the text for N_2 and O_2 and their reference atoms with similar I_p Ar and Xe. The region with weak intensity dependence identifies NSDI suggesting an intensity regime of roughly $1.5-4\times10^{14}\,\mathrm{W\,cm^{-2}}$ for N_2 and $0.4-1\times10^{14}\,\mathrm{W\,cm^{-2}}$ for O_2 at 800 nm. Part **b** shows the same plot for CO_2 using linear (*LP*) and circular polarisation (*CP*) indicating an NSDI regime for $0.5-2\times10^{14}\,\mathrm{W\,cm^{-2}}$ at 800 nm (Reprinted with permission from [93] and [97]. Copyright (1998) and (2010) by the American Physical Society)

corresponding plots are displayed in Fig. 2.16. In this case, NSDI was identified by the intensity dependence of the ratio X^{2+}/X^{+}, where X refers to the molecule. For a nonsequential process X^{+} is an intermediate state. Therefore the intensity dependence of the above ratio should be weak. For sequential ionisation on the other hand, X^{+} is a precursor state and hence the corresponding ratio should have a strong intensity dependence as this would lead to a depletion of the X^{+} yield along with and increase of the X^{2+} yield. Furthermore, the results show that in N_2 NSDI is pronounced the most and in O_2 the least. The authors attribute this to the open shell structure of O_2, with the two outermost electrons occupying different but degenerate orbitals. This would lead to a lower probability of removing both in a non-sequential process. CO_2 on the other hand has a closed shell structure (the outermost $1\pi_g$ orbital is fully filled with four electrons), but the two electrons can either be removed from different (degenerate) or the same orbital [97]. Following the author's arguments, this would explain the higher NSDI rate compared to O_2 and lower compared to N_2, where the two electrons will always come from the same fully filled ($3\sigma_g^2$) orbital.

Due to their rich nuclear structure, several additional laser-molecule interactions can take place and restrain the observation of the different NSDI channels. The most important ones in the context of this thesis are the influence of the molecular orbital asymmetry on the first ionisation step and dynamic alignment effects. Available experimental results are briefly reviewed in the following sections.

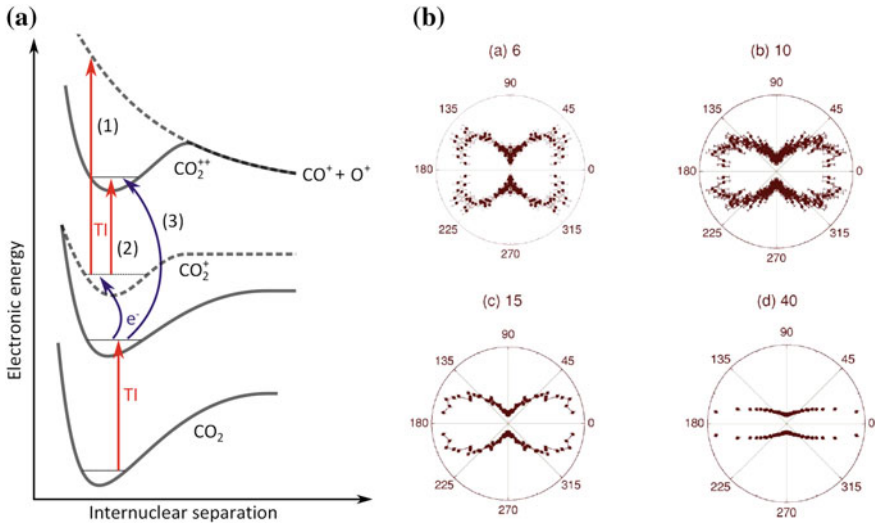

Fig. 2.17 **a** Graphical representation of possible pathways in molecular NSDI with CO_2 as example. *Dashed* PECs denote excited states, TI refers to tunneling ionisation and e^- to recollision. (*1*) RESI to a repulsive state of CO_2^{++} resulting in two charged fragments. (*2*) RESI to a bound state of CO_2^{++}. (*3*) (e, 2e) channel to a bound CO_2^{++} state. **b** Angularly resolved relative yields of channel (*1*) from the *left panel*. For all measurements the laser polarisation is *horizontal* and for each plot the estimated peak intensity is denoted in $10^{13}\,\mathrm{W\,cm^{-2}}$ (Part **b** reprinted with permission from [99]. Copyright (2005) by the American Physical Society)

2.4.1 Molecular Structure Effects

The crucial effect of the molecular geometry and associated orbitals is its impact on ionisation probability, as mentioned already in Sect. 2.3.1. In particular, Alnaser et al. [98, 99] measured the angular distributions of ion fragments, created in a dissociative double ionisation of several di- and triatomic molecules. Here, CO_2 is treated as an example. The authors focussed on dissociation channels with two singly charged fragments in order to reconstruct the initial molecular alignment from the fragment's momentum vectors detected in coincidence. This is illustrated as channel (1) in part (a) of Fig. 2.17, which also displays the RESI and (e, 2e) channels in the molecular potential energy curve picture. Part (b) of Fig. 2.17 then shows the experimental angular distributions for different intensities. Here, 8 fs pulses at 790 nm were employed in the NSDI intensity regime. At the lowest intensity a clear maximum at approximately 40° with respect to the laser polarisation along the y-axis can be observed. This agrees well with the angular distribution of TI in CO_2 (see Fig. 2.14) and thus suggests that it is mainly the angular dependence from the first ionisation step that determines the angular distribution of the overall process. Similar results were found for the other molecules and are in very good agreement with theoretical predictions and earlier studies [95].

2.4.2 Laser Induced Alignment Effects

There are two types of alignment of the molecular geometry in the laboratory frame, which can alter the angular distribution of ion fragments: *dynamic alignment* (DA) or non-adiabatic alignment (for details see Chap. 5) describing the molecule's laser induced reorientation before the dissociation, due to its dipole moment and *post-ionisation alignment* (PIA), which describes a deflection of the ion fragments in the presence of the laser pulse due the molecular polarizability [100, 101].

Both effects depend on an interplay between the polarisability or induced dipole moment of the molecule, its mass and the pulse length (at a given intensity). For heavy molecules like I_2 DA can generally be neglected [100, 102]. For lighter molecules, Alnaser et al. [99] showed that the effect can be neglected for example in CO_2 for short pulses around 8 fs and low intensities at $6 \times 10^{13}\,\mathrm{W\,cm^{-2}}$. This was confirmed by a study by Tong [101] and Voss [103] in O_2, which additionally showed that PIA cannot be neglected for 35 fs pulses but does not play a role at 8 fs and low intensities. While it is not easy to disentangle the DA and PIA, their impact can be observed in the angular fragment distributions in part (b) of Fig. 2.17. For increasing intensity, the distribution becomes increasingly confined around the laser polarisation direction.

2.4.3 NSDI in Aligned Diatomics

In order to determine the influence of the molecular structure on the recollision step, one has to disentangle it from the ionisation and propagation step, which is possible when performing measurements on NSDI in the molecular frame. Using COLTRIMS, the molecular frame is reconstructed from the momentum vectors of the fragments. It is thus not possible to employ this approach when detecting doubly ionised molecules directly. For this, Zeidler et al. [39] used COLTRIMS together with non-adiabatic alignment to probe the molecules in their frame of reference. It was found that for the molecule being aligned along the laser polarisation, NSDI is slightly more probable and the RESI channel less pronounced. One important aspect of Zeidler's experiment is a possible route to the removal of the ionisation step by determining the single ionisation yield of N_2 prior to the main experiment and thus determining the NSDI yields as ratios of double and single ionisation yields. In order to take any kind of fluctuations into account, the relative alignment-dependent single ionisation yields were determined from a Ne/N_2 gas mixture, where the Ne yield works as a reference. In this way 19 % more N_2^+ and 30 % more N_2^{++} ions were observed for parallel molecules at $(1.2 \pm 0.2) \times 10^{14}\,\mathrm{Wcm^{-2}}$. This is in good agreement with a similar experiment performed by Litvinyuk et al. where the N_2^+ yield was 23 % higher for parallel aligned molecules at $2 \times 10^{14}\,\mathrm{Wcm^{-2}}$ [104].

Zeidler's findings are in agreement with several theoretical studies [83, 105, 106]. Jia et al. [83] use an S-Matrix approach to calculate alignment-dependent ratios of N_2^{++}/N_2^+ taking into account the initial ionisation probability and the probability of the first ionised electron being driven back to the ion. The authors attribute the alignment-dependence of the NSDI yield to the corresponding dependence of

the ionisation cross section of N_2^+. The authors suggest that the angularly resolved recollision cross section scales like the electron density profile of the parent ion. Furthermore, the authors also find that the influence of lower lying orbitals must be included to obtain a better agreement with the experimental data.

2.5 Recollision Induced Fragmentation

Recollision induced fragmentation (RIF) takes place when the molecular ion is excited to a repulsive state via electron impact ionisation or excitation. RIF can be divided into a dissociative excitation (DE) and dissociation ionisation channel (DI) (see channel (1) in part (a) of Fig. 2.17). In DE the parent ion is excited to a dissociative state (see part (a) in Fig. 2.18), whereas in DI the parent ion is ionised further, such that the higher charged ion fragments. The recollision contribution to such mechanisms is studied significantly less intensively than NSDI, but its qualitative behaviour under a change of laser parameters is expected to be similar. In this section, experimental results obtained in small and large molecules are briefly reviewed.

2.5.1 Small Molecules

DE has so far been observed in CO_2 [27] and N_2 [26] and O_2 [107]. DI has been observed in N_2 and O_2 [96, 107, 108]. In the case of CO_2 McKenna et al. suggest that RIF is responsible for a significant DE enhancement for linear compared to circular polarisation [27]. The results are displayed in part (b) of Fig. 2.18. Here, recollision is switched off for circular polarisation, while the intensity is adjusted to match the effective ionisation rate for both polarisation states (see Sect. 2.1.2). With the same arguments, RIF could be identified in the (1, 0) channel in N_2 [26], even though the results are probably only reliable at low intensities, where molecular alignment effects of the driving laser field were weak.

The angular distributions of DE and DI in O_2 were studied recently with a COLTRIMS [107]. As expected, the distributions qualitatively follow the single ionisation rate distribution, yet DE is peaked around 30° and DI around 40°. This is an interesting result pointing towards a significant influence of the recollision step in these processes.

Wu et al. [108, 109] have studied the polarisation dependence of the DI channel in N_2 and O_2 in passively aligned molecules. This means that in the experiment the detection geometry restricted the collection to molecules aligned along one axis in the laboratory frame. Recollision was identified via the intensity dependence of the X^{2+}/X^+ ratio explained in the Sect. 2.5 and compared for parallel and perpendicular polarisation with respect to the molecular bond. It was found that for parallel polarisation, recollision induced DI is significantly suppressed in O_2.

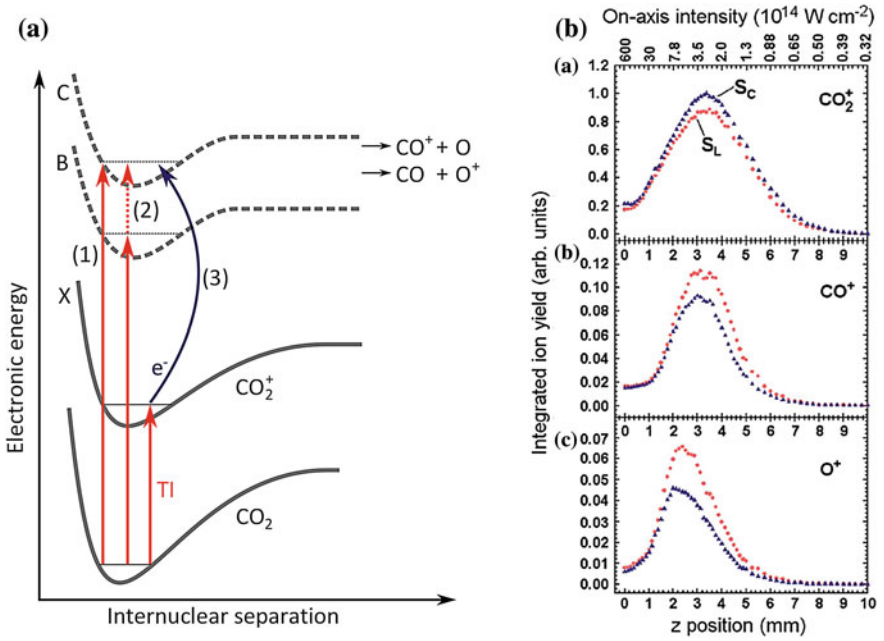

Fig. 2.18 **a** possible dissociative excitation pathways in CO_2. *Dashed* PECs denote excited states, TI refers to tunneling ionisation and e^- to recollision. Note that only the C state is above the relevant dissociation limits. (*1*) direct TI, (*2*) TI to B state and photoexciation (*dotted arrow*) to C state, (*3*) TI followed by recollision induced excitation to C state. **b** Ion yields in CO_2 as a function of intensity for linear (*red circles*) and circular (*blue triangles*) polarisations using 55 fs, 790 nm pulses. Even though the single ionisation rate is not perfectly matched, a clear enhancement for linear polarisation is visible (Part **b** reprinted with permission from [27]. Copyright (2006) by the American Physical Society)

2.5.2 Large Molecules

RIF has been observed as a significant mechanism in the alkanes methane, ethane and propane [110–112], water [112], in the relatively small organic molecule benzene [112, 113], in a series of alcohols [114] and in C_60 [115]. Yet its contribution has also been shown to be negligible in typical organic molecules like anthracene [116] and naphtalene [117].

In the experiment by Rajgara et al. [114] a series of alcohols of increasing size was investigated using pulses at 800 nm, 100 fs, 10^{16} W cm^{-2}. Recollision was shown to be the dominant fragmentation mechanism by observing a significant suppression of the fragmentation yields, when using circular polarisation. The high intensity was chosen, as experiments on benzene by Talebpour et al. with pulses at 800 nm, 100 fs, 10^{15} W cm^{-2} did not show such a suppression and hence ruled out recollision as a mechanism [118]. Other than investigating this threshold intensity (and thus recollision energy) the impact of the molecular structure of the differently sized

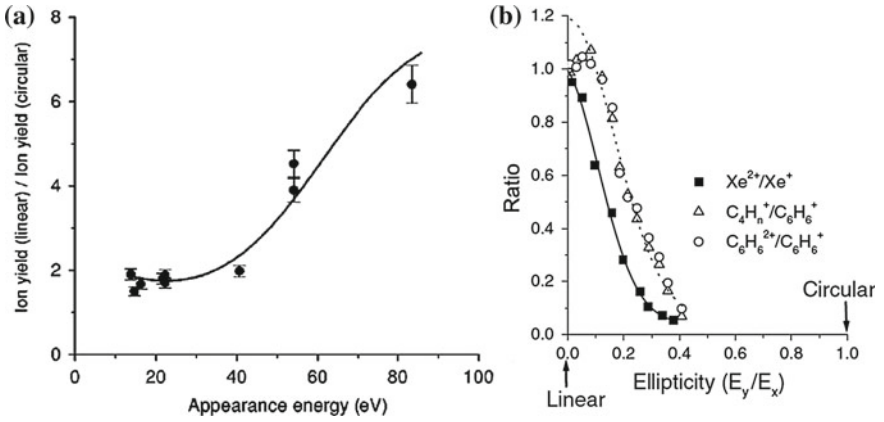

Fig. 2.19 **a** Impact of the molecular structure in differently sized alkohols on recollision induced fragmentation. Here, the ratio of fragment ion yield at *linear* to the yield at *circular* polarisation is displayed as a function of appearance energy. This energy is a measure of the energy transfer to the molecule required to produce the corresponding fragment ion. **b** Ellipticity dependence of fragmentation of benzene (Part **a** reproduced with permission from [114]. Copyright (2003), AIP Publishing LLC. Part **b** reprinted with permission from [113]. Copyright (2001) by the American Physical Society)

alcohols was investigated. By measuring the relative suppression of several fragments corresponding to different appearance energies, the authors concluded that suppression and hence recollision induced fragmentation was most dominant for the fragmentation channels which require the highest energy transfer to the cation. The corresponding data is displayed in part (a) of Fig. 2.19.

In another series of measurements with the same setup, Rajgara and coworkers confirmed these results in the molecules water, methanol and benzene [112]. In addition to the above measurements at very high intensity, a lower bound of $2.0 \times 10^{15}\,\mathrm{W\,cm^{-2}}$ (379 eV) was found for recollision induced fragmentation in benzene. This is only marginally higher than in Talebpour's experiment and explains, why it was not observed then. It should be noted however that a few details remain open in the above experiments. It is for example not clear how big the impact of the peak intensity variation on the recorded yields is, when switching from linear to circular polarisation. This is because the intensity was kept constant throughout the experiment. The authors also point out to be above the saturation intensity of the investigated molecules, which means that the effective peak intensity acting on the recolliding electron remains unknown. Furthermore the fragmentation event upon recollision was not investigated further, such that it is not clear whether an excitation to a dissociative state or an impact fragmentation was present.

Bhardwaj et al. [113] then observed recollision induced fragmentation in benzene by increasing the recollision energy to 401 eV via a longer wavelength of 1400 nm, compared to 189 eV in Talebpour's experiment [118]. This has the advantage of staying below the saturation intensity of the molecule. The pulse length was 70 fs, with an intensity of $7 \times 10^{14}\,\mathrm{W\,cm^{-2}}$ on target. Recollision induced fragmentation

was identified by observing the same ellipticity dependence for the fragmentation and NSDI channels. The corresponding data is displayed in part (b) of Fig. 2.19. Furthermore the fragmentation and NSDI yields have an unexpected maximum at an ellipticity of about 0.1. This is interpreted by the authors as follows. A nodal plane aligned along the linear laser polarisation direction leads to a recolliding wavepacket with non-zero transverse momentum, driving it away from the polarization direction and hence the parent ion. However, in an elliptical driving laser field, the transverse field component may compensate for the electron's initial momentum. This manifests itself in a maximum NSDI yield for nonzero laser ellipticity. Due to the large number of broad nodal planes in the HOMO of C_6H_6, this effect is expected to be visible even in a randomly oriented sample. A similar explanation has been used to explain the absence of recollision induced effects in CS_2 [119].

References

1. A. Einstein, Über einen die erzeugung und verwandlung des lichtes betreffenden heuristischen gesichtspunkt. Annalen der Physik **322**(6), 132–148 (1905)
2. G.S. Voronov, N.B. Delone, Sov. Phys. JETP Lett. **1**, 66 (1965)
3. C.H.K.M Protopapas, P.L. Knight, Atomic physics with super-high intensity lasers. Rep. Prog. Phys. **60**, 389 (1997)
4. P. Agostini, F. Fabre, G. Mainfray, G. Petite, N.K. Rahman, Free-free transitions following six-photon ionization of xenon atoms. Phys. Rev. Lett. **42**, 1127–1130 (1979)
5. F. Fabre, G. Petite, P. Agostini, M. Clement, Multiphoton above-threshold ionisation of xenon at 0.53 and 1.06 μ m. J. Phys. B: At. Mol. Phys. **15**(9), 1353–1369 (1982)
6. T. Brabec, *Strong Field Laser Physics* (Springer, Berlin, 2008)
7. L.A. Lompré, A. L'Huillier, G. Mainfray, C. Manus, Laser-intensity effects in the energy distributions of electrons produced in multiphoton ionization of rare gases. J. Opt. Soc. Am. B: Opt. Phys. **2**, 1906–1912 (1985)
8. G.G. Paulus, W. Nicklich, H. Walther, Investigation of above-threshold ionization with femtosecond pulses: connection between plateau and angular distribution of the photoelectrons. Europhys. Lett. (EPL) **27**, 267–272 (1994)
9. G.G. Paulus, W. Nicklich, H. Xu, P. Lambropoulos, H. Walther, Plateau in above threshold ionization spectra. Phys. Rev. Lett. **72**, 2851–2854 (1994)
10. L. Keldysh, Ionization in the field of a strong electromagnetic wave. Sov. Phys. JETP **20**, 1314, 1307 (1965)
11. T. Brabec, F. Krausz, Intense few-cycle laser fields: frontiers of nonlinear optics. Rev. Mod. Phys. **72**, 545 (2000)
12. F. Krausz, M. Ivanov, Attosecond physics. Rev. Mod. Phys. **81**, 163 (2009)
13. G.L. Yudin, M.Y. Ivanov, Nonadiabatic tunnel ionization: looking inside a laser cycle. Phys. Rev. A **64**, 013409 (2001)
14. F.H.M. Faisal, Multiple absorption of laser photons by atoms. J. Phys. B: At. Mol. Phys. **6**, L89–L92 (1973)
15. H.R. Reiss, Effect of an intense electromagnetic field on a weakly bound system. Phys. Rev. A **22**, 1786–1813 (1980)
16. M. Lewenstein, P. Balcou, M.Y. Ivanov, A. L'Huillier, P.B. Corkum, Theory of high-harmonic generation by low-frequency laser fields. Phys. Rev. A **49**, 2117 (1994)
17. A.M. Perelomov, V.S. Popov, M.V. Terent'ev, Ionization of atoms in an alternating electric field. Sov. J. Exp. Theor. Phys. **23**, 924 (1966)
18. A.M. Perelomov, V.S. Popov, M.V. Terent'ev, Ionization of atoms in an alternating electric field: II. Sov. J. Exp. Theor. Phys. **24**, 207 (1967)

19. A.M. Perelomov, V.S. Popov, Ionization of atoms in an alternating electrical field. III. Sov. J. Exp. Theor. Phys. **25**, 336 (1967)
20. N.B.D.M.V. Ammosov, V.P. Krainov, Tunnel ionization of complex atoms and atomic ions by an alternating electromagnetic field. Sov. Phys. JETP **64**, 1191–1194 (1986)
21. S.F.J. Larochelle, A. Talebpour, S.L. Chin, Coulomb effect in multiphoton ionization of rare-gas atoms. J. Phys. B: At. Mol. Opt. Phys. **31**, 1215–1224 (1998)
22. P.B. Corkum, Plasma perspective on strong field multiphoton ionization. Phys. Rev. Lett. **71**, 1994–1997 (1993)
23. C. Cornaggia, P. Hering, Nonsequential double ionization of small molecules induced by a femtosecond laser field. Phys. Rev. A **62**(2), 023403 (2000)
24. M.Y. Ivanov, M. Spanner, O. Smirnova, Anatomy of strong field ionization. J. Mod. Opt. **52**, 165–184 (2005)
25. M. Suresh, J. McKenna, B. Srigengan, I. Williams, E. English, S. Stebbings, W. Bryan, W. Newell, E. Divall, C. Hooker, A. Langley, Multiple ionization of ions and atoms by intense ultrafast laser pulses. Nucl. Instrum. Methods Phys. Res. Sect. B **235**(1–4), 216–220 (2005)
26. J. McKenna, M. Suresh, B. Srigengan, I.D. Williams, W.A. Bryan, E.M.L. English, S.L. Stebbings, W.R. Newell, I.C.E. Turcu, J.M. Smith, E.J. Divall, C.J. Hooker, A.J. Langley, J.L. Collier, Ultrafast ionization study of N_2 in intense linearly and circularly polarized laser fields. Phys. Rev. A **73**(4), 043401 (2006)
27. J. McKenna, M. Suresh, B. Srigengan, I.D. Williams, W.A. Bryan, E.M.L. English, S.L. Stebbings, W.R. Newell, I.C.E. Turcu, J.M. Smith, E.J. Divall, C.J. Hooker, A.J. Langley, J.L. Collier, Rescattering-enhanced dissociation of a molecular ion. Phys. Rev. A **74**, 043409 (2006)
28. B. Zon, Tunneling ionization of atoms with excitation of the core. J. Exp. Theor. Phys. **91**(5), 899–904 (2000)
29. M. Lezius, V. Blanchet, D.M. Rayner, D.M. Villeneuve, A. Stolow, M.Y. Ivanov, Nonadiabatic multielectron dynamics in strong field molecular ionization. Phys. Rev. Lett. **86**, 51 (2001)
30. W.A. Bryan, S.L. Stebbings, J. McKenna, E.M.L. English, M. Suresh, J. Wood, B. Srigengan, I.C.E. Turcu, J.M. Smith, E.J. Divall, C.J. Hooker, A.J. Langley, J.L. Collier, I.D. Williams, W.R. Newell, Atomic excitation during recollision-free ultrafast multi-electron tunnel ionization. Nat. Phys. **2**(6), 379–383 (2006)
31. A.N. Pfeiffer, C. Cirelli, M. Smolarski, R. Dörner, U. Keller, Timing the release in sequential double ionization. Nat. Phys. **7**(5), 428–433 (2011)
32. A.N. Pfeiffer, C. Cirelli, M. Smolarski, X. Wang, J.H. Eberly, R. Drner, U. Keller, Breakdown of the independent electron approximation in sequential double ionization. New J. Phys. **13**, 093008 (2011)
33. I.V. Litvinyuk, F. Logar, P.W. Dooley, D.M. Villeneuve, P.B. Corkum, J. Zanghellini, A. Pegarkov, C. Fabian, T. Brabec, Shakeup excitation during optical tunnel ionization. Phys. Rev. Lett. **94**, 033003 (2005)
34. Z.B. Walters, O. Smirnova, Attosecond correlation dynamics during electron tunnelling from molecules. J. Phys. B: At. Mol. Opt. Phys. **43**(16), 161002 (2010)
35. G.G. Paulus, W. Becker, W. Nicklich, H. Walther, Rescattering effects in above-threshold ionization: a classical model. J. Phys. B: At. Mol. Opt. Phys. **27**, L703–L708 (1994)
36. M. Lein, Molecular imaging using recolliding electrons. J. Phys. B: At. Mol. Opt. Phys. **40**(16), R135–R173 (2007)
37. K.C. Kulander, K.J. Schafer, J.L. Krause, Super-intense laser-atom physics, in *NATO Advanced Study Institute Series B: Physics*, vol. 316 (Plenum, New York, 1993), p. 95
38. R. Thomson, C. Leburn, D. Reid (eds.), *Ultrafast Nonlinear Optics* (Springer, Berlin, 2013)
39. D. Zeidler, A. Staudte, A.B. Bardon, D.M. Villeneuve, R. Dorner, P.B. Corkum, Controlling attosecond double ionization dynamics via molecular alignment. Phys. Rev. Lett. **95**, 203003 (2005)
40. K.S. Budil, P. Salires, M.D. Perry, A. L'Huillier, Influence of ellipticity on harmonic generation. Phys. Rev. A **48**, R3437 (1993)

41. J. Guo, T. Wang, X.-S. Liu, J.-Z. Sun, Non-sequential double ionization of mg atoms in elliptically polarized laser fields. Laser Phys. **23**, 055303 (2013)
42. T. Brabec, M.Y. Ivanov, P.B. Corkum, Coulomb focusing in intense field atomic processes. Phys. Rev. A **54**(4), R2551–R2554 (1996)
43. X. Wang, J.H. Eberly, Elliptical trajectories in nonsequential double ionization. New J. Phys. **12**, 093047 (2010)
44. J. Tate, T. Auguste, H.G. Muller, P. SaliTres, P. Agostini, L.F. DiMauro, Scaling of wave-packet dynamics in an intense midinfrared field. Phys. Rev. Lett. **98**, 013901 (2007)
45. S. Augst, D. Strickland, D.D. Meyerhofer, S.L. Chin, J.H. Eberly, Tunneling ionization of noble gases in a high-intensity laser field. Phys. Rev. Lett. **63**, 2212 (1989)
46. T. Auguste, P. Monot, L.A. Lompre, G. Mainfray, C. Manus, Multiply charged ions produced in noble gases by a 1 ps laser pulse at lambda = 1053 nm. J. Phys. B: At. Mol. Opt. Phys. **25**(20), 4181 (1992)
47. D.N. Fittinghoff, P.R. Bolton, B. Chang, K.C. Kulander, Observation of nonsequential double ionization of helium with optical tunneling. Phys. Rev. Lett. **69**, 2642 (1992)
48. U. Eichmann, M. Dörr, H. Maeda, W. Becker, W. Sandner, Collective multielectron tunneling ionization in strong fields. Phys. Rev. Lett. **84**, 3550 (2000)
49. E. Eremina, Electron correlation in multiple ionization of atoms and molecules by intense ultra-short laser pulses. Ph.D. thesis, TU Berlin (2005)
50. D.N. Fittinghoff, P.R. Bolton, B. Chang, K.C. Kulander, Polarization dependence of tunneling ionization of helium and neon by 120-fs pulses at 614 nm. Phys. Rev. A **49**, 2174 (1994)
51. O. Herrwerth, A. Rudenko, M. Kremer, V.L.B. de Jesus, B. Fischer, G. Gademann, K. Simeonidis, A. Achtelik, T. Ergler, B. Feuerstein, C.D. Schrter, R. Moshammer, J. Ullrich, Wavelength dependence of sub-laser-cycle few-electron dynamics in strong-field multiple ionization. New J. Phys. **10**(2), 025007 (2008)
52. B. Feuerstein, R. Moshammer, D. Fischer, A. Dorn, C.D. Schrter, J. Deipenwisch, J.R.C. Lopez-Urrutia, C. Hhr, P. Neumayer, J. Ullrich, H. Rottke, C. Trump, M. Wittmann, G. Korn, W. Sandner, Separation of recollision mechanisms in nonsequential strong field double ionization of Ar: the role of excitation tunneling. Phys. Rev. Lett. **87**, 043003 (2001)
53. R. Moshammer, B. Feuerstein, W. Schmitt, A. Dorn, C. D. Schröter, J. Ullrich, H. Rottke, C. Trump, M. Wittmann, G. Korn, K. Hoffmann, W. Sandner, Momentum distributions of Ne^{n+} ions created by an intense ultrashort laser pulse. Phys. Rev. Lett. **84**, 447 (2000)
54. R. Moshammer, J. Ullrich, B. Feuerstein, D. Fischer, A. Dorn, C.D. Schrter, J.R.C. Lpez-Urrutia, C. Hhr, H. Rottke, C. Trump, M. Wittmann, G. Korn, K. Hoffmann, W. Sandner, Strongly directed electron emission in non-sequential double ionization of ne by intense laser pulses. J. Phys. B: At. Mol. Opt. Phys. **36**(6), L113–L119 (2003)
55. A. Rudenko, T. Ergler, K. Zrost, B. Feuerstein, V.L.B. de Jesus, C.D. Schrter, R. Moshammer, J. Ullrich, From non-sequential to sequential strong-field multiple ionization: identification of pure and mixed reaction channels. J. Phys. B: At. Mol. Opt. Phys. **41**(8), 081006 (2008)
56. R. Dörner, V. Mergel, O. Jagutzki, L. Spielberger, J. Ullrich, R. Moshammer, H. Schmidt-Bcking, Cold target recoil ion momentum spectroscopy: a 'momentum microscope' to view atomic collision dynamics. Phys. Rep. **330**, 95–192 (2000)
57. A. Rudenko, K. Zrost, B. Feuerstein, V.L.B. de Jesus, C. D. Schröter, R. Moshammer, J. Ullrich, Correlated multielectron dynamics in ultrafast laser pulse interactions with atoms. Phys. Rev. Lett. **93**, 253001 (2004)
58. V.L.B. de Jesus, B. Feuerstein, K. Zrost, D. Fischer, A. Rudenko, F. Afaneh, C.D. Schröter, R. Moshammer, J. Ullrich, Atomic structure dependence of nonsequential double ionization of He, Ne and Ar in strong laser pulses. J. Phys. B: At. Mol. Opt. Phys. **37**(8), L161–L167 (2004)
59. A.S. Alnaser, D. Comtois, A.T. Hasan, D.M. Villeneuve, J. Kieffer, I.V. Litvinyuk, Strong-field non-sequential double ionization: wavelength dependence of ion momentum distributions for neon and argon. J. Phys. B: At. Mol. Opt. Phys. **41**(3), 031001 (2008)
60. X. Liu, H. Rottke, E. Eremina, W. Sandner, E. Goulielmakis, K.O. Keeffe, M. Lezius, F. Krausz, F. Lindner, M.G. Schtzel, G.G. Paulus, H. Walther, Nonsequential double ionization at the Single-Optical-Cycle limit. Phys. Rev. Lett. **93**, 263001 (2004)

61. S. Baker, J.S. Robinson, C.A. Haworth, H. Teng, R.A. Smith, C.C. Chiril, M. Lein, J.W.G. Tisch, J.P. Marangos, Probing proton dynamics in molecules on an attosecond time scale. Science **312**(5772), 424–427 (2006)
62. J.I. Steinfeld, *Molecules and Radiation: Introduction to Modern Molecular Spectroscopy* (MIT Press, Cambridge, 1978)
63. D. Tannor, *Introduction to Quantum Mechanics: A Time-Dependent Perspective*, U.S., illustrated edn. (University Science Books, Sausalito, 2007)
64. H. Lefebvre-Brion, R.W. Field, *The Spectra and Dynamics of Diatomic Molecules: Revised and Enlarged Edition*, 1st edn. (Academic Press, New York, 2004)
65. W. Demtrder, *Atoms, Molecules and Photons: An Introduction to Atomic- Molecular- and Quantum Physics* (Springer, Berlin, 2005)
66. P.B. Bransden, P.C. Joachain, *Physics of Atoms and Molecules*, 2nd edn. (Prentice Hall, Harlow, 2003)
67. M.J. Winter, *Chemical Bonding* (Oxford University Press, Oxford,1994)
68. P. Atkins, R. Friedman, *Molecular Quantum Mechanics*, 4th edn. (Oxford University Press, Oxford, 2005)
69. Bandrauk, *Molecules in Laser Fields*, 1st edn. (CRC Press, Boca Raton, 1993)
70. J. Franck, E.G. Dymond, Elementary processes of photochemical reactions. Trans. Faraday Soc. **21**, 536 (1926)
71. E.U. Condon, Nuclear motions associated with electron transitions in diatomic molecules. Phys. Rev. **32**, 858–872 (1928)
72. J.H. Posthumus, The dynamics of small molecules in intense laser fields. Rep. Prog. Phys. **67**(5), 623–665 (2004)
73. L.J. Frasinski, J.H. Posthumus, J. Plumridge, K. Codling, P.F. Taday, A.J. Langley, Manipulation of bond hardening in H_2^+ by chirping of intense femtosecond laser pulses. Phys. Rev. Lett. **83**, 3625–3628 (1999)
74. L.J. Frasinski, J. Plumridge, J.H. Posthumus, K. Codling, P.F. Taday, E.J. Divall, A.J. Langley, Counterintuitive alignment of H_2^+ in intense femtosecond laser fields. Phys. Rev. Lett. **86**, 2541–2544 (2001)
75. P.H. Bucksbaum, A. Zavriyev, H.G. Muller, D.W. Schumacher, Softening of the H_2^+ molecular bond in intense laser fields. Phys. Rev. Lett. **64**, 1883–1886 (1990)
76. A. Giusti-Suzor, F.H. Mies, Vibrational trapping and suppression of dissociation in intense laser fields. Phys. Rev. Lett. **68**, 3869–3872 (1992)
77. J.J. Larsen, Laser induced alignment of neutral molecules. Ph.D. thesis, Institute of Physics and Astronomy, University of Aarhus, Denmark (2000)
78. K. Codling, L.J. Frasinski, Coulomb explosion of simple molecules in intense laser fields. Contemp. Phys. **35**(4), 243 (1994)
79. M. Abu-samha, L.B. Madsen, Theory of strong-field ionization of aligned Co_2. Phys. Rev. A **80**(2), 023401 (2009)
80. X.M. Tong, Z.X. Zhao, C.D. Lin, Theory of molecular tunneling ionization. Phys.Rev. A **66**(3), 033402 (2002)
81. B.K. McFarland, J.P. Farrell, P.H. Bucksbaum, M. Guhr, High harmonic generation from multiple orbitals in N_2. Science **322**, 1232–1235 (2008)
82. W. Boutu, S. Haessler, H. Merdji, P. Breger, G. Waters, M. Stankiewicz, L.J. Frasinski, R. Taieb, J. Caillat, A. Maquet, P. Monchicourt, B. Carre, P. Salieres, Coherent control of attosecond emission from aligned molecules. Nat. Phys. **4**(7), 545–549 (2008)
83. X. Jia, W. Li, J. Liu, J. Chen, Alignment-dependent nonsequential double ionization of N_2 in intense laser fields: the role of different valence orbitals. Phys. Rev. A **80**, 053405 (2009)
84. O. Smirnova, Y. Mairesse, S. Patchkovskii, N. Dudovich, D. Villeneuve, P. Corkum, M.Y. Ivanov, High harmonic interferometry of multi-electron dynamics in molecules. Nature **460**(7258), 972–977 (2009)
85. D. Pavicic, K.F. Lee, D.M. Rayner, P.B. Corkum, D.M. Villeneuve, Direct measurement of the angular dependence of ionization for N_2, O_2, and Co_2 in intense laser fields. Phys. Rev. Lett. **98**(24), 243001 (2007)

86. G.A. Gallup, I.I. Fabrikant, Semiclassical complex-time method for tunneling ionization: molecular suppression and orientational dependence. Phys. Rev. A **81**(3), 033417 (2010)
87. S. Petretti, Y.V. Vanne, A. Saenz, A. Castro, P. Decleva, Alignment-dependent ionization of N_2, O_2, and Co_2 in intense laser fields. Phys. Rev. A **104**(22), 223001 (2010)
88. R. Murray, M. Spanner, S. Patchkovskii, M.Y. Ivanov, Tunnel ionization of molecules and orbital imaging. Phys. Rev. A **106**(17), 173001 (2011)
89. L. Torlina, M. Ivanov, Z.B. Walters, O. Smirnova, Time-dependent analytical R-matrix approach for strong-field dynamics. II. many-electron systems. Phys. Rev. A **86**, 043409 (2012)
90. S.M. Hankin, D.M. Villeneuve, P.B. Corkum, D.M. Rayner, Nonlinear ionization of organic molecules in high intensity laser fields. Phys. Rev. Lett. **84**, 5082 (2000)
91. S.M. Hankin, D.M. Villeneuve, P.B. Corkum, D.M. Rayner, Intense-field laser ionization rates in atoms and molecules. Phys. Rev. A **64**, 013405 (2001)
92. T. Koopmans, Über die zuordnung von wellenfunktionen und eigenwerten zu den einzelnen elektronen eines atoms. Physica **1**(16), 104–113 (1934)
93. C. Guo, M. Li, J.P. Nibarger, G.N. Gibson, Single and double ionization of diatomic molecules in strong laser fields. Phys. Rev. A **58**, R4271 (1998)
94. A. Rudenko, B. Feuerstein, K. Zrost, V.L.B. de Jesus, T. Ergler, C. Dimopoulou, C.D. Schrter, R. Moshammer, J. Ullrich, Fragmentation dynamics of molecular hydrogen in strong ultrashort laser pulses. J. Phys. B: At. Mol. Opt. Phys. **38**(5), 487–501 (2005)
95. E. Eremina, X. Liu, H. Rottke, W. Sandner, M.G. Schuetzel, A. Dreischuh, G.G. Paulus, H. Walther, R. Moshammer, J. Ullrich, Influence of molecular structure on double ionization of N_2 and O_2 by high intensity ultrashort laser pulses. Phys. Rev. Lett. **92**, 173001 (2004)
96. C. Guo, G.N. Gibson, Ellipticity effects on single and double ionization of diatomic molecules in strong laser fields. Phys. Rev. A **63**(4), 040701 (2001)
97. L. Pei, C. Guo, Nonsequential double ionization of triatomic molecules in strong laser fields. Phys. Rev. A **82**(2), 021401 (2010)
98. A.S. Alnaser, X.M. Tong, T. Osipov, S. Voss, C.M. Maharjan, P. Ranitovic, B. Ulrich, B. Shan, Z. Chang, C.D. Lin, C.L. Cocke, Routes to control of H_2 coulomb explosion in few-cycle laser pulses. Phys. Rev. Lett. **93**, 183202 (2004)
99. A.S. Alnaser, C.M. Maharjan, X.M. Tong, B. Ulrich, P. Ranitovic, B. Shan, Z. Chang, C.D. Lin, C.L. Cocke, I.V. Litvinyuk, Effects of orbital symmetries in dissociative ionization of molecules by few-cycle laser pulses. Phys. Rev. A **71**, 031403 (2005)
100. P. Dietrich, D.T. Strickland, M. Laberge, P.B. Corkum, Molecular reorientation during dissociative multiphoton ionization. Phys. Rev. A **47**, 2305 (1993)
101. X.M. Tong, Z.X. Zhao, A.S. Alnaser, S. Voss, C.L. Cocke, C.D. Lin, Post ionization alignment of the fragmentation of molecules in an ultrashort intense laser field. J. Phys. B: At. Mol. Opt. Phys. **38**(4), 333–341 (2005)
102. C. Ellert, P.B. Corkum, Disentangling molecular alignment and enhanced ionization in intense laser fields. Phys. Rev. A **59**, R3170 (1999)
103. S. Voss, A.S. Alnaser, X. Tong, C. Maharjan, P. Ranitovic, B. Ulrich, B. Shan, Z. Chang, C.D. Lin, C.L. Cocke, High resolution kinetic energy release spectra and angular distributions from double ionization of nitrogen and oxygen by short laser pulses. J. Phys. B: At. Mol. Opt. Phys. **37**(21), 4239–4257 (2004)
104. I. Litvinyuk, Alignment-dependent strong field ionization of molecules. Phys. Rev. Lett. **90**, 233003 (2003)
105. J. Liu, D.F. Ye, J. Chen, X. Liu, Complex dynamics of correlated electrons in molecular double ionization by an ultrashort intense laser pulse. Phys. Rev. Lett. **99**, 013003 (2007)
106. Y. Li, J. Chen, S.P. Yang, J. Liu, Alignment effect in nonsequential double ionization of diatomic molecules in strong laser fields. Phys. Rev. A **76**(2), 023401 (2007)
107. X. Liu, C. Wu, Z. Wu, Y. Liu, Y. Deng, Q. Gong, Recollision-induced dissociation and ionization of oxygen in few-cycle laser fields. Phys. Rev. A **83**(3), 035403 (2011)
108. J. Wu, H. Zeng, C. Guo, Polarization effects on nonsequential double ionization of molecular fragments in strong laser fields. Phys. Rev. A **75**, 043402 (2007)

109. C. Guo, M. Li, J.P. Nibarger, G.N. Gibson, Nonsequential double ionization of molecular fragments. Phys. Rev. A **61**(3), 033413 (2000)
110. Z. Wu, C. Wu, Q. Liang, S. Wang, M. Liu, Y. Deng, Q. Gong, Fragmentation dynamics of methane by few-cycle femtosecond laser pulses. J. Chem. Phys. **126**, 074311 (2007)
111. C. Wu, Z. Wu, Q. Liang, M. Liu, Y. Deng, Q. Gong, Ionization and dissociation of alkanes in few-cycle laser fields. Phys. Rev. A **75**, 043408 (2007)
112. F.A. Rajgara, M. Krishnamurthy, D. Mathur, Electron rescattering and the fragmentation dynamics of molecules in strong optical fields. Phys. Rev. A **68**(2), 023407 (2003)
113. V.R. Bhardwaj, D.M. Rayner, D.M. Villeneuve, P.B. Corkum, Quantum interference in double ionization and fragmentation of C_6H_6 in intense laser fields. Phys. Rev. Lett. **87**, 253003 (2001)
114. F.A. Rajgara, M. Krishnamurthy, D. Mathur, Electron rescattering and the dissociative ionization of alcohols in intense laser light. J. Chem. Phys. **119**(23), 12224 (2003)
115. V.R. Bhardwaj, P.B. Corkum, D.M. Rayner, Recollision during the high laser intensity ionization of C_{60}. Phys. Rev. Lett. **93**, 043001 (2004)
116. M. Murakami, M. Tanaka, T. Yatsuhashi, N. Nakashima, Enhancement of anthracene fragmentation by circularly polarized intense femtosecond laser pulse. J. Chem. Phys. **126**(10), 104304 (2007)
117. T. Yatsuhashi, N. Nakashima, Formation and fragmentation of quadruply charged molecular ions by intense femtosecond laser pulses. J. Phys. Chem. A **114**, 7445–7452 (2010)
118. A. Talebpour, A.D. Bandrauk, K. Vijayalakshmi, S.L. Chin, Dissociative ionization of benzene in intense ultra-fast laser pulses. J. Phys. B: At. Mol. Opt. Phys. **33**(21), 4615 (2000)
119. D. Mathur, A.K. Dharmadhikari, F.A. Rajgara, J.A. Dharmadhikari, Molecular symmetry effects in the ionization of CS_2 by intense, few-cycle laser pulses (2008), arXiv:0801.2046v1

http://www.springer.com/978-3-319-05337-0

Resolving Strong Field Dynamics in Cation States of CO_2 via Optimised Molecular Alignment

Oppermann, M.

2014, XVIII, 205 p. 94 illus., 37 illus. in color., Hardcover
ISBN: 978-3-319-05337-0